American Mineralogist, Volume 107, pages 1519–1531, 2022

Trace element partitioning between olivine and melt in lunar basalts

Sha Chen[1], Peng Ni[1], Youxue Zhang[1,*], and Joel Gagnon[2]

[1]Department of Earth and Environmental Sciences, University of Michigan, Ann Arbor, Michigan 48109, U.S.A.
[2]School of the Environment, University of Windsor, Windsor, Ontario N9B 3P4, Canada

Abstract

Mineral/melt partition coefficients have been widely used to provide insights into magmatic processes. Olivine is one of the most abundant and important minerals in the lunar mantle and mare basalts. Yet, no systematic olivine/melt partitioning data are available for lunar conditions. We report trace element partition data between host mineral olivine and its melt inclusions in lunar basalts. Equilibrium is evaluated using the Fe-Mg exchange coefficient, leading to the choice of melt inclusion-host olivine pairs in lunar basalts 12040, 12009, 15016, 15647, and 74235. Partition coefficients of 21 elements (Li, Mg, Al, Ca, Ti, V, Cr, Mn, Fe, Co, Y, Zr, Nb, Gd, Tb, Dy, Ho, Er, Tm, Yb, and Lu) were measured. Except for Li, V, and Cr, these elements show no significant difference in olivine-melt partitioning compared to the data for terrestrial samples. The partition coefficient of Li between olivine and melt in some lunar basalts with low Mg# (Mg# < 0.75 in olivine, or < ~0.5 in melt) is higher than published data for terrestrial samples, which is attributed to the dependence of D_{Li} on Mg# and the lack of literature D_{Li} data with low Mg#. The partition coefficient of V in lunar basalts is measured to be 0.17 to 0.74, significantly higher than that in terrestrial basalts (0.003 to 0.21), which can be explained by the lower oxygen fugacity in lunar basalts. The significantly higher D_V can explain why V is less enriched in evolved lunar basalts than terrestrial basalts. The partition coefficient of Cr between olivine and basalt melt in the Moon is 0.11 to 0.62, which is lower than those in terrestrial settings by a factor of ~2. This is surprising because previous authors showed that Cr partition coefficient is independent of f_{O_2}. A quasi-thermodynamically based model is developed to correlate Cr partition coefficient to olivine and melt composition and f_{O_2}. The lower Cr partition coefficient between olivine and basalt in the Moon can lead to more Cr enrichment in the lunar magma ocean, as well as more Cr enrichment in mantle-derived basalts in the Moon. Hence, even though Cr is typically a compatible element in terrestrial basalts, it is moderately incompatible in primitive lunar basalts, with a similar degree of incompatibility as V based on partition coefficients in this work, as also evidenced by the relatively constant V/Cr ratio of 0.039 ± 0.011 in lunar basalts. The confirmation of constant V/Cr ratio is important for constraining concentrations of Cr (slightly volatile and siderophile) and V (slightly siderophile) in the bulk silicate Moon.

Keywords: Partition coefficients, lunar basalts, olivine, melt inclusions, Cr/V ratio

Introduction

Mineral/melt partition coefficients have been widely used to provide insights into magmatic processes. Olivine is one of the most abundant and important minerals in the lunar mantle and mare basalts. Olivine fractionation in the lunar magma ocean (LMO) and during lunar basalt differentiation plays a significant role in the evolution of the magma (Wood et al. 1970; Longhi 1977; Solomon and Longhi 1977; Snyder et al. 1992; Elardo et al. 2011; Lin et al. 2017; Charlier et al. 2018; Rapp and Draper 2018). Olivine-melt partitioning also plays a role in controlling the composition of mantle-derived basalts. Hence, quantifying olivine-melt partitioning is critical to understanding and modeling magma evolution of the LMO and lunar basalts.

Although numerous partitioning studies have been published for olivine and basaltic melt, they show significant variability for most elements due to the wide range of compositions, conditions, and methods involved. For example, the Ti partition coefficient between olivine and melt varies by more than two orders of magnitude, ranging from 0.0019 to 0.43 (Duke 1976; Rollinson 1993; McDade et al. 2003; Spandler and O'Neill 2010; Papike et al. 2013; Laubier et al. 2014; Burnham and O'Neill 2016; Leitzke et al. 2016). In addition, these studies often focus on terrestrial samples and physicochemical conditions. Though lunar and terrestrial basalts share many similarities in terms of their chemical composition, they are distinct in several aspects. Compared to typical terrestrial basalts, lunar basalts have highly variable TiO_2, lower Al_2O_3 and alkalis, and often higher FeO and Cr_2O_3 concentrations. For example, terrestrial basalts rarely contain ≥5 wt% TiO_2 in the melt due to Fe-Ti oxide saturation at ~1100 °C (Toplis and Carroll 1995), whereas lunar basalts may contain up to 14 wt% TiO_2. Such compositional differences have been shown to affect the physical properties of the melt, metal solubility in silicate melts (Borisov et al. 2004), and mineral/melt partition coefficients of

* E-mail: youxue@umich.edu. Orcid 0000-0002-7439-0086

0003-004X/22/0008–1519$05.00/DOI: https://doi.org/10.2138/am-2022-7971

multiple elements (Xirouchakis et al. 2001; Dygert et al. 2013; Leitzke et al. 2016). Another important difference between lunar and terrestrial conditions that might affect elemental partitioning behavior is the oxygen fugacity (f_{O_2}). The f_{O_2} has been estimated to be approximately IW-1 for the lunar mantle and basalts (Sato et al. 1973; Wadhwa 2008), but ~QFM for the terrestrial upper mantle (O'Neill et al. 2018), representing a difference of over four orders of magnitude. Therefore, partition coefficients for multivalent elements, such as V, Cr, Fe, and Ti, could be significantly different under lunar conditions.

Chen et al. (2015) and Ni et al. (2017, 2019) have published a data set of major element concentrations in melt inclusions and their olivine hosts, as well as trace element data in melt inclusions in several lunar basalts. In this study, we supplement the data of Ni et al. (2019) with trace element measurements in olivine to estimate their partition coefficients. We also examine new olivine-melt inclusion pairs in lunar basalt 12009. Here we report partition coefficients of 21 major and trace elements between olivine and melt in lunar basalts and compare the obtained partition coefficients with published data for terrestrial conditions.

Samples and methods

General considerations

The compositions of a homogenized melt inclusion (MI) and its host olivine can be used to estimate mineral/melt partition coefficients. A melt inclusion is a droplet of melt that becomes trapped during mineral crystallization. At the time of entrapment, a melt inclusion can be considered to be in equilibrium with the host mineral. If well-preserved, coexisting host minerals and melt inclusions can be analyzed to estimate partition coefficients (e.g., Nikogosian and Sobolev 1997; Thomas et al. 2002; Zajacz and Halter 2007) and may have advantages over experimental methods. For example, naturally occurring, coeval host mineral/melt inclusions reflect natural composition and conditions and, therefore, can more accurately represent geological processes.

This method, however, also has its disadvantages. The compositions of melt inclusions can be affected during natural cooling, including post-entrapment crystallization and diffusive exchange between the melt inclusion and the host crystal as well as the magma surrounding the host crystal. Post-entrapment crystallization of the host mineral into the melt inclusion as well as the crystallization of the melt inclusion during cooling is supposed to be reversed (corrected for) by laboratory homogenization, which was carried out for all melt inclusions in this study. Whether homogenization reverses post-entrapment crystallization can be evaluated by whether equilibrium is reached for Fe-Mg exchange between a given melt inclusion and its host olivine. Diffusive exchange occurs during cooling between melt inclusions and magma surrounding the host olivine or between the melt inclusion and olivine. The extent of exchange depends on the cooling rate, diffusivity, and compatibility of the element, size of the olivine host and melt inclusion, and residence time of the host crystal in the magma. A significant diffusive exchange between a melt inclusion and melt surrounding the host olivine would occur when the cooling rate is 1 to 2 °C/year or lower (Gaetani and Watson 2000, 2002). All lunar samples investigated in this work cooled at >10 °C/h (see "Sample description and preparation" section), which is 4 to 5 orders of magnitude faster than 1 to 2 °C/year. Furthermore, most of the samples reported here (except 12009) have been examined for volatile concentrations (Ni et al. 2019), which showed, with the exception of H_2O, preservation of rapidly diffusing components, such as F, Cl, and S. Such observations indicate a negligible diffusive exchange for the elements examined here, which, with the exception of Li, diffuse more slowly than F (e.g., Zhang et al. 2010).

All melt inclusions studied in this work were crystalline. Naturally glassy melt inclusions (such as those in 74220 studied by Hauri et al. (2011), Chen et al. (2015), and Ni et al. (2019)] did not satisfy our selection criterion. Therefore, homogenization was needed. For homogenization experiments, it is difficult to completely restore the MI composition to that at the time of entrapment (i.e., equilibrium). Therefore, a criterion is needed to assess whether there is approximate equilibrium between the melt inclusion and the host olivine. The Fe/Mg exchange coefficient K_D [= $(FeO/MgO)_{olivine}/(FeO/MgO)_{melt}$] between olivine and basaltic melt was used to evaluate whether there is approximate olivine-melt equilibrium.

Roeder and Emslie (1970) first showed that the Fe^{2+}-Mg exchange coefficient between olivine and melt is independent of temperature and equals 0.30 ± 0.03 at equilibrium. This exchange coefficient has been widely used in equilibrium calculations ever since (e.g., Langmuir et al. 1980). Longhi et al. (1978), using lunar samples, reached a similar conclusion but noted decreasing K_D with increasing TiO_2. Xirouchakis et al. (2001) further studied the effect of TiO_2 concentration in melt and found that K_D can vary from 0.36 to 0.22 with a TiO_2 increase from <1 to 20 wt%. From the data summarized in Xirouchakis et al. (2001), an equation showing this dependence was fitted ($K_D = -0.006668 \times TiO_2 + 0.35$) and used in this work. We allowed a variation of ±0.06 (~20% relative) in K_D from the calculated value in choosing olivine-inclusion pairs thought to be in equilibrium. Using this criterion, we have chosen previously investigated lunar samples 12040, 15016, 15647, and 74235 (Ni et al. 2019) for trace element measurement in olivine. In addition, a new lunar sample (12009) that we investigated also satisfied the criterion and was included in this study.

Sample description and preparation

Olivine-melt inclusion pairs in five lunar basalts, 12009, 12040, 15016, 15647, and 74235, satisfy the criterion for equilibrium based on the apparent K_D between the host olivine and melt inclusion and were analyzed to obtain olivine-melt partition coefficients. Among the five lunar samples, four (all except 12009) were examined for volatiles in olivine-hosted melt inclusions by Ni et al. (2019). One sample (74235) is a high-Ti basalt, and the other four samples are low-Ti basalts. A brief description of each sample is presented here. Sample 12040 is an olivine basalt with millimeter-sized crystals and ~2.6 wt% TiO_2. Accumulation of olivine was inferred for the sample (Newton et al. 1971). Sample 15016 is an olivine-normative basalt with ~2.3 wt% TiO_2 and ~50 vol% vesicularity. Ca- or Fe-rich zonation in pyroxene indicates rapid crystallization. Sample 15647 is an olivine basalt with sub-millimeter size crystals and containing ~2.4 wt% TiO_2. Sample 74235 is a fine-grained high-Ti basalt (~12.3 wt% TiO_2) containing skeletal phenocrysts of olivine, pyroxene, and ilmenite. Sample 12009 is a rapidly cooled low-Ti (3.3 wt% TiO_2) olivine vitrophyre basalt with large vesicles. More detailed descriptions of these samples can be found in The Lunar Sample Compendium (https://curator.jsc.nasa.gov/lunar/lsc/) and Ni et al. (2019).

Cooling rates of 74235, 12009, and 12040 have been estimated and are all greater than 10 °C/h (Donaldson et al. 1975; Usselman et al. 1975; Walker et al. 1976). For 15016 and 15647, no cooling rate data are available. Based on the H_2O/Ce ratio vs. cooling rate relation in Ni et al. (2019), they should have quenched faster than 12040, meaning a cooling rate greater than 10 °C/h. Hence, all lunar samples we studied cooled much more rapidly than 2 °C/year, with 12040 cooling the slowest, and 15647 a close second.

The radii of the investigated melt inclusions range from 13 to 22.5 μm (Table 1). Grain sizes in crystalline melt inclusions are typically small, sub-micrometers to a few micrometers for silicate minerals (Fig. 1 and Newton 1971), but there might be larger metal or oxide mineral grains (brighter crystals in the lower right of Fig. 1), and shrinkage bubbles.

Homogenization experiments were conducted at 1 bar at a temperature slightly above the liquidus of the corresponding lunar rock. The olivine-hosted melt inclusions in 12040, 15016, 15647, and 74235 were homogenized by Ni et al. (2019), and those in sample 12009 were homogenized in this study following the procedures in Chen et al. (2015) and Ni et al. (2017, 2019). An olivine grain from 12009 was placed in a graphite crucible (drilled from purified 99.995% graphite rod ordered from graphitestore.com) under continuous high-purity N_2 flow to maintain a reducing environment, heated to 1240 to 1250 °C at one bar for 2 min, and quickly quenched by immersing the crucible in water. The f_{O_2} in the crucible was measured to be between IW-1.9 and IW-2.6 (Ni et al. 2017). The reducing condition prevented olivine oxidation but did not establish a new f_{O_2} for the olivine-inclusion equilibrium due to the short duration of the experiments. That is, the f_{O_2} condition is expected to be unchanged from that during eruption and crystallization on the Moon. More detailed description of the homogenization experiments may be found in Chen et al. (2015) and Ni et al. (2017, 2019).

The homogenized melt inclusions are essentially glassy (Fig. 2), but occasionally there are undissolved metal/sulfide/oxide grains. Silicate crystals of a few micrometers in size or smaller can be dissolved in ≤10 s at the experimental temperatures (Chen and Zhang 2008, 2009). Diffusion distance $(Dt)^{1/2}$ (here D is diffusivity, not partition coefficient) in a MORB melt during olivine dissolution at the experimental temperature for 2 min is 41 μm for MgO and 24 μm for the slower diffusing SiO_2 and Al_2O_3 using diffusivities in Chen and Zhang (2008). Diffusivities in lunar basalts are higher than those in MORB by a factor of about 4 (Morgan et al. 2006; Yu et al. 2016), meaning diffusion distances would be two times those in MORB, which equate to approximately 82 μm for MgO and 48 μm for SiO_2 and Al_2O_3. All melt inclusions in this study have radii smaller than 23 μm (Table 1). Hence, diffusion is able to homogenize the melt inclusions in 2 min except for the

TABLE 1. Trace element concentration (ppm) for olivine and MI with 1σ error

	74235-4				12040-36				12040-41				12009-6				12009-11				15016-10				15647-6			
	OL4	1σ	MI	1σ	OL36	1σ	MI	1σ	OL41	1σ	MI	1σ	OL6	1σ	MI	1σ	OL11	1σ	MI	1σ	OL10	1σ	MI	1σ	OL6	1σ	MI	1σ
Diameter (μm)	240		45		274		28		153		31		146*450		35		300		20*33		517		29		443		40	
Mg#	71.5		34.3		44.9		23.4		57.4		34.2		73.3		44.1		73.5		42.5		70.3		44.6		45.5		19.7	
Li	4.28	0.31	7.70	0.29	7.97	0.54	5.10	0.14	8.91	0.61	4.80	0.13	2.85	0.15			2.69	0.14			2.37	0.13	2.70	0.21	7.19	0.36	6.20	0.15
Na			3667	33			3065	9			3484	10											2092	16			1996	7.50
Al	312	8.75	EMP		81.7	3.20	EMP		84	3.49	EMP		248	4.12	EMP		254	4.11	EMP		222	3.89	EMP		83.6	2.03	EMP	
K			614	8			635	5			718	6											209	6			580	5.2
Ti	809	46.1	EMP		329	19.9	EMP		321	20	EMP		193	7.83	EMP		203	8.14	EMP		145	6	EMP		383	15.3	EMP	
V	33.1	0.97	141	5	10.2	0.33	30	1.0	35	1.09	63	0.8	90	1.71	123	8.1	91.2	1.71	123	19.0	93.9	1.8	141.6	0.4	18.95	0.47	111	1.0
Cr	1318	74	5169	64	344	21	1735	60	753	45	2516	24	2883	115	4629	205	2851	113	4730	482	2654	107	8835	13	460	21	4308	16
Mn	2220	56	3223	40	3159	80	2129	22	2676	75	2161	19	1998	35	2132	72	1975	34	2251	173	2059	37	2860	3	3977	85	3891	27
Co	52.4	2.5	23.0	2.3	87.5	3.91	22	1.0	105	4.79	21	1	116	3.59	70	8.1	115	3.55	6460	17.0	113	3.5	28.0	0.5	113	3.72	129	2.00
Sr			177	3			128	1.3			145	1.3											93.0	2.3			105	1.2
Y	0.53	0.02	102	1	10.47	0.33	501	1.2	1.92	0.076	197	1	0.267	0.009			0.28	0.01			0.18	0.01	29.3	0.6	0.89	0.03	43.6	0.4
Zr	0.129	0.006	254	2	0.17	0.01	161	1.1	0.080	0.004	183	1	0.071	0.003			0.08	0.00			0.05	0.00	101	2	0.09	0.00	83.0	1.2
Nb	0.004	0.0004	28.1	0.7			9.9	0.3	0.003	3E-04	11.7	0.3	0.00391	3E-04			0.005	0.0003			0.005	0.0004	7.2	0.45	0.004	0.0004	10.9	0.3
Ba			65	3			85.0	0.3			95.0	0.3											42.0	3.50			80.0	0.3
La			6.5	0.3			9.40	0.23			9.50	0.23											5.30	0.36			9.80	0.24
Ce			25.9	0.7			28.6	0.43			27.3	0.4											15.7	0.68			25.7	0.4
Pr			4.4	0.3			5.50	0.17			4.40	0.15											2.00	0.21			3.80	0.14
Nd			23.6	1			40.1	0.75			24.4	0.6											12.2	0.85			19.7	0.5
Sm			8.4	0.9			27.3	0.94			10.9	0.6											4.10	0.67			6.50	0.46
Eu			3.0	0.7			1.90	0.49			1.20	0.44											0.74	0.70			0.60	0.40
Gd	0.015	0.0011	12	1	0.293	0.016	53.9	1.3	0.044	0.003	18.2	0.7	0.00779	5E-04			0.008	0.0004			0.006	0.0004	4.8	0.8	0.044	0.0026	7.6	0.5
Tb	0.006	0.0003	2.7	0.2	0.117	0.005	12.9	0.3	0.023	0.001	4.5	0.2	0.00253	1E-04			0.003	0.0001			1E-03	6E-05	0.9	0.2	0.011	0.0005	1.4	0.1
Dy	0.065	0.0035	19.6	0.7	1.278	0.054	95.6	0.9	0.223	0.011	33.8	0.5	0.02822	0.001			0.033	0.0013			0.02	0.0009	6.4	0.5	0.105	0.0044	8.4	0.3
Ho	0.02	0.001	3.9	0.3	0.381	0.014	20.0	0.4	0.074	0.003	7.7	0.2	0.00977	4E-04			0.01	0.0003			0.006	0.0002	1.2	0.2	0.036	0.0013	1.6	0.1
Er	0.079	0.0041	10.8	0.6	1.456	0.062	52.0	0.8	0.26	0.013	20.9	0.5	0.04051	0.002			0.049	0.0019			0.032	0.0013	3.4	0.4	0.142	0.0056	4.8	0.2
Tm	0.021	0.0009	1.8	0.2	0.291	0.01	5.8	0.2	0.046	0.002	2.6	0.12	0.01032	3E-04			0.01	0.0003			0.008	0.0003	0.4	0.1	0.025	0.0009	0.6	0.1
Yb	0.164	0.0076	11.2	0.5	2.178	0.082	36.8	0.6	0.404	0.018	15.7	0.4	0.10299	0.003			0.095	0.0032			0.055	0.002	2.8	0.3	0.22	0.0079	3.7	0.2
Lu	0.038	0.0015	1.4	0.2	0.361	0.012	4.8	0.2	0.075	0.003	2.4	0.2	0.01937	6E-04			0.02	0.0006			0.009	0.0003	0.6	0.2	0.047	0.0015	0.44	0.07

Notes: Concentration data and associated errors in melt inclusion for 74235-4,12040-36, 12040-41, 15016-10, and 15647-6 Are from Ni et al. (2019).

presence of larger grains of metal or oxide or sulfide.

After homogenization, the olivine crystals were polished to reveal the enclosed melt inclusions (Fig. 2). The diameter of each melt inclusion was measured and reported in Table 1. Major and trace element concentrations in both melt inclusions and host mineral grains were analyzed.

Major and trace element concentration measurement

Major element analysis. Major element concentrations of melt inclusions and host olivine grains were analyzed using a CAMECA SX-100 electron microprobe (EMPA) at the University of Michigan. Analyses were carried out using a 15 kV, 10 nA, and 5 μm defocused beam in wavelength-dispersive spectrometry (WDS) mode. At least five points were measured on the host olivine at locations adjacent to each melt inclusion. Fewer data points were obtained for some melt inclusions due to the limitation of their small sizes. Data are reported in Table 2 (all tables are in an Excel file for easy use by readers in Online Materials[1]). We only report olivine-melt inclusion pairs that were considered to be approximately in equilibrium based on their apparent Fe^{2+}-Mg K_D values.

Trace element concentrations in melt inclusions. Trace element concentrations in melt inclusions were analyzed using secondary ion mass spectrometry (SIMS) at the California Institute of Technology using a Cameca IMS 7f- GEO. Trace element measurements for sample 12009 were conducted in this study, while those for lunar samples 12040, 15016, 15647, and 74235 are from Ni et al. (2019). The analytical procedures are very similar and briefly described below.

Twenty-two trace elements (Li, Na, K, Sr, Y, Zr, Nb, Ba, La, Ce, Pr, Nd, Sm, Eu, Gd, Tb, Dy, Ho, Er, Tm, Yb, Lu) and four transition metal elements (V, Cr, Mn, Co) were analyzed in two separate sessions. For the analyses of trace elements, a 10 to 13 nA O^- primary ion beam was used to generate secondary ion signals for measurement. Sensitivity factors were calculated using the internal standard of ^{30}Si based on reported concentrations in NIST glass standard SRM 610 (Pearce et al. 1997). Accuracy of the analyses was verified by measuring two additional NIST standards (NIST 612 and NIST 614) and two MPI-DING glass standards (GOR128-G and KL2-G). For the analyses of transition metal elements, an 11 to 17 nA O^- primary ion beam was used and a mass resolution power (MRP) of 5500 was applied to the mass spectrometer to separate interferences from the target masses.

Most data on olivine-hosted melt inclusions are from Ni et al. (2019), and the calibration curves are shown and discussed there. Calibration curves for the transition metal elements for 12009 can be found in Online Materials[1] Figure S5. Calculated concentrations in standards in this work are compared with reference values (Jochum et al. 2005, 2006, 2011) in Online Materials[1] Figure S6 and Online Materials[1] Table S2. Nickel concentrations were also measured, but the measured concentrations in some standards can differ from reference values by more than a factor of 4. Hence, Ni data are not used.

Trace element concentrations in olivine. Trace element analyses for all olivine crystals reported in this study were carried out using a laser ablation-inductively coupled plasma-mass spectrometry (LA-ICP-MS) system in the Element and Heavy Isotope Analytical Laboratories at the University of Windsor. The instrumentation comprises a Photon Machines Analyte Excite 193 nm, short (sub 4 ns) pulse width Ar-F Excimer laser ablation system coupled with an Agilent 7900, fast scanning quadrupole ICP-MS. For each LA-ICP-MS analysis, 30 s of gas and instrument background were acquired with the laser off, followed by 40 s ablation signal with the laser on. The laser was operated at a pulse energy of 120 mJ and a repetition rate of 5 Hz, with 60% output power. Three spot sizes, 50, 85, and 110 μm, were applied depending on the olivine crystal size.

Most trace elements are highly incompatible in olivine relative to the coexisting silicate melt, thus leading to their extremely low concentrations. The concentrations of Na, K, La, Ce, Pr, Nd, Sm, Eu, Nb, Mo, and Sn in olivine were found to be below the detection limit. Nonetheless, 18 trace elements (using isotopes of ^7Li, ^{27}Al, ^{49}Ti, ^{51}V, ^{52}Cr, ^{55}Mn, ^{59}Co, ^{89}Y, ^{90}Zr, ^{93}Nb, ^{157}Gd, ^{159}Tb, ^{163}Dy, ^{165}Ho, ^{166}Er, ^{169}Tm, ^{172}Yb, and ^{175}Lu) were successfully measured, and their concentrations

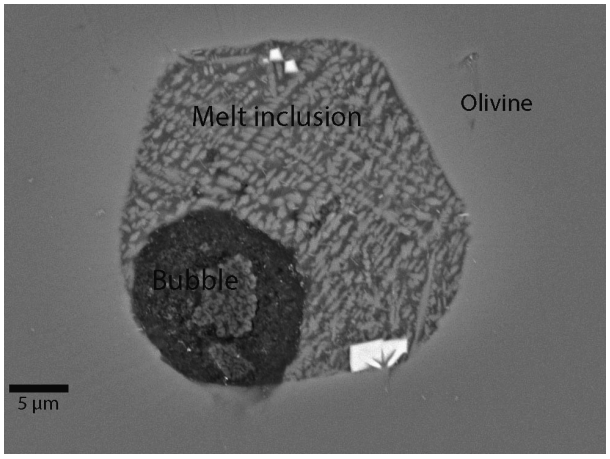

Figure 1. BSE image of a crystalline melt inclusion in olivine in lunar sample 12009 with a bubble (12009-OL1-MI1) without homogenization.

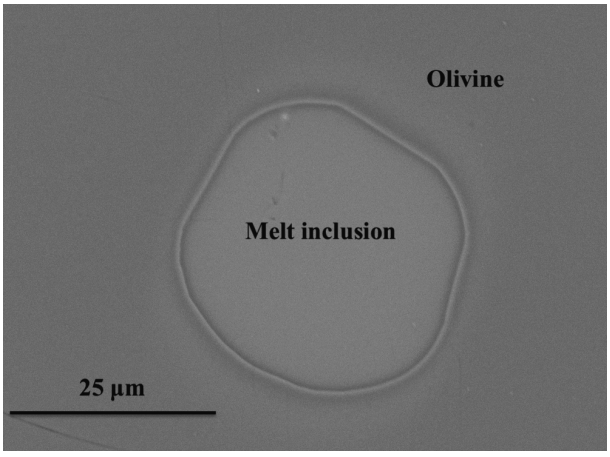

Figure 2. BSE image of a homogenized melt inclusion in olivine in 12009 (12009-OL6-MI1).

with 1σ errors are reported in Table 1. When possible, two isotopes per element (^{6}Li and ^{7}Li, ^{47}Ti and ^{49}Ti, ^{52}Cr and ^{53}Cr, ^{60}Ni and ^{62}Ni, ^{66}Zn and ^{68}Zn, ^{90}Zr and ^{91}Zr, ^{95}Mo and ^{98}Mo, ^{116}Sn, ^{118}Sn, and ^{119}Sn) were measured to check for reproducibility and mass interferences.

NIST standards 610, 612, 614, and 616 plus three MPI-DING standards (GOR128-G, GOR132-G, St-Hs-G) were used as external calibration standards. The NIST standards are soda-lime silicate glasses doped with various concentration levels of trace elements. NIST 610, 612, 614, and 616 are nominally doped with approximately 500, 50, 1, and 0.02 ppm, respectively, of most trace elements. Since all the aforementioned standards contain more than 1 wt% Al, a SRM 1830 glass with a low-Al concentration (635 ppm, certified), similar to the olivine samples, was used for LA-ICP-MS calibration. ^{29}Si was used as the internal calibration standard to correct for differences in the rate of ablation between the standards and olivine crystals.

Inclusions were avoided during LA-ICP-MS measurements both by positioning the laser spot away from visible inclusions and by assessing each spectrum for evidence of compositional change in olivine. Calibration curves are shown in Online Materials[1] Figures S1, S2, and S3 for beam diameters of 65, 85, and 110 µm, respectively. When there is significant scatter in the calibration curve for a given element (e.g., Ge, Zn, and Sc in Online Materials[1] Figure S1), the calibration is deemed unacceptable and elemental concentrations in samples are not calculated. The concentrations in the standards obtained in this study are compared with reference values (GeoRem, Jochum et al. 2005, 2006, 2011) in Online Materials[1] Figure S4 and Online Materials[1] Table S2.

Results

Comparison of melt inclusion and whole rock composition

Melt inclusions in olivine crystals studied here have a range of SiO_2 concentrations from 38.0 to 48.3 wt% and the Mg# range of the host olivine is 0.45 to 0.74. Three samples (15016, 74235, and 12009) have olivine Mg# (or Fo#) >0.70, while samples 12040 and 15647 with slower cooling rate have low-olivine Mg# ranging from 0.45 to 0.57.

Major oxide concentrations in melt inclusions for 74235, 15016, and 12009 are generally consistent with the whole rock. On the other hand, melt inclusions in 12040 are considerably different in composition from the whole rock, especially in MgO (4 to 6 wt% in MIs vs. ~16 wt% in whole rock, The Lunar Sample Compendium), which is consistent with the accumulation of olivine in the whole rock of 12040 (e.g., Newton et al. 1971). The high

Table 2. Major element concentrations for olivine and melt inclusions (MIs) measured by EMPA

		SiO_2	1σ	TiO_2	1σ	Al_2O_3	1σ	Cr_2O_3	1σ	FeO	1σ	MnO	1σ	MgO	1σ	CaO	1σ
74235	OL4	38.62187	0.19	0.139878	0.04	0.0552	0.04	0.241422	0.05	25.26317	0.10	0.290044	0.01	35.58591	0.30	0.284411	0.01
	MI	38.0	0.3	12.5	0.2	8.18	0.15			22.16	0.26	0.31	0.02	6.53	0.34	9.95	0.24
	WR	38.6–39.4		12.2–12.4		8.61–9.21		0.42–0.51		18.6–19.3		0.27–0.28		8.35–8.67		10.7–10.9	
12040	OL36	33.15084	0.19	0.06642	0.04	0.02264	0.02	0.0547	0.03	44.43224	0.37	0.40438	0.02	20.28716	0.49	0.36754	0.03
	MI	46.3	0.2	3.08	0.14	8.42	0.25			25.3	0.1	0.27	0.00	4.34	0.35	9.42	0.22
	WR	43.4–44.9		2.27–2.78		6.67–7.8		0.52–0.71		19.7–23		0.24–0.28		16.1–17.1		6.9–8.1	
12040	OL41	35.5961	0.47	0.056333	0.03	0.0151	0.01	0.111633	0.05	36.6691	0.34	0.3527	0.02	27.70987	0.36	0.323667	0.02
	MI	46.5	0.2	3.68	0.00	10.60	0.17			20.3	0.0	0.23	0.03	5.94	0.27	11.10	0.03
	WR	43.4–44.9		2.27–2.78		6.67–7.8		0.52–0.71		19.7–23		0.24–0.28		16.1–17.1		6.9–8.1	
12009	OL6	38.73828	0.15	0.03714	0.01	0.03294	0.02	0.46298	0.02	23.98956	0.37	0.2173	0.02	36.96392	0.29	0.2882	0.01
	MI	45.8	0.2	3.4	0.1	10.4	0.2			17.3	0.3			7.7	0.4	11.7	0.2
	WR	41–45.0		2.9–3.3		8.59–11				20–21.0		0.19–0.28		11.6–12.5		9.42–10	
12009	OL11	38.3118	0.09	0.03456	0.03	0.04422	0.02	0.4592	0.04	23.7218	0.06	0.2418	0.01	36.87296	0.14	0.27576	0.01
	MI	47.4	0.48	3.46	0.20	10.3	0.36	0.65	0.05	17.4	0.43	0.24	0.02	7.20	0.57	11.5	0.16
	WR	41–45.0		2.9–3.3		8.59–11				20–21.0		0.19–0.28		11.6–12.5		9.42–10	
15016	OL10	37.92441	0.21	0.039171	0.01	0.029914	0.01	0.319257	0.14	26.65424	0.40	0.274286	0.02	35.39361	0.34	0.313271	0.02
	MI	48.3	0.3	1.94	0.13	9.12	0.43			19.04	0.55	0.24	0.02	8.6	0.9	10.4	0.3
	WR	43.8–44.3		2.1–3		8.17–8.8				16.5–23.0		0.26–0.33		11–11.7		9.06–10.9	
15647	OL6	34.32505	0.43	0.066575	0.01	0.011425	0.01	0.109575	0.04	44.0175	0.98	0.433675	0.03	20.60805	0.92	0.40915	0.04
	MI	42.12	0.38	3.24	0.06	6.71	21.00			32.8	0.5	0.35	0.02	4.53	0.26	8.16	0.26
	WR	44.4–46.2		2.35–3		7.86–9				22.2–23.9		0.26–0.29		10.0–10.5		8.8–9.67	

Notes: The major element concentrations in melt inclusion for 74235-4, 12040-36, 12040-41, 15016-10, and 15647-6 are from Ni et al. (2019). OL, MI, and WR represent the concentration in olivine crystal, melt inclusion, and whole rock. Whole rock composition from The Lunar Sample Compendium is listed for comparison. Errors (1σ) are reported based on the standard deviation of multiple measurements.

FeO in olivine (36.7 and 44.4 wt%) indicates late crystallization or re-equilibration during the relatively slow cooling process (The Lunar Sample Compendium).

Another slowly cooled basalt, 15647, also contains high FeO (43.9 wt%) in olivine. The melt inclusion investigated here is enriched in FeO by ~10 wt% and depleted in MgO by ~5 wt% and SiO_2 by ~3 wt% compared with the whole rock. The high-FeO concentrations in both the olivine host and the melt inclusion in sample 15647 indicate a more evolved composition than the whole rock.

Partition coefficients between olivine and melt

Partition coefficients and associated errors (1σ) between olivine and lunar basalt are reported in Table 3. Errors are calculated using the equation:

$$\sigma_D = D * \sqrt{\left(\frac{\sigma_X}{X}\right)^2 + \left(\frac{\sigma_Y}{Y}\right)^2}$$

(X and Y are the concentrations in the mineral and melt inclusion, respectively). In general, Mg and Co behave compatibly in olivine. Fe, Mn, and Li exhibit close to neutral compatibility. V and Cr are moderately incompatible in olivine, while most other elements (Al, Ca, Ti, Y, Zr, Nb, and REEs) are highly incompatible.

To examine whether the variation of partition coefficients is mainly due to data scatter, such as measurement uncertainty or disequilibrium, partition coefficients of different elements are plotted vs. each other, and good correlations are found between element pairs such as REE-Y, Y-Ti, Ca-Ti, Cr-Ca, and Li-Al (Fig. 3). As a dominant major element in olivine, the Mg partition coefficient has a narrow range (4.12 to 5.45). Hence, no obvious correlation was found between D_{Mg} and the partition coefficients of any other element. There is excellent correlation among REE and Y partition coefficients (Fig. 3a). Furthermore, the partition coefficients of REE increase with D_{Ca} and D_{Ti} (Figs. 3b and 3c), and the partition coefficients of V and Cr decrease with increasing D_{Ca} and D_{Ti} (Figs. 3d and 3e). The partition coefficient of Al is negatively correlated with that of Li (Fig. 3f).

The correlations in Figure 3 indicate that, at least for the elements shown, the variation of the partition coefficients is not due to measurement uncertainty or disequilibrium. Specifically, the good correlation between D_{Li} and D_{Al} indicates that D_{Li} is not significantly affected by disequilibrium due to post-entrapment diffusion. The most likely cause for the variation is compositional dependence. Hence, we examined the dependence of the partition coefficients on melt composition by plotting D vs. various oxide concentrations in the melt. The dependence of partition coefficients on TiO_2 in the melt is not obvious, partially because there is only one high-Ti basalt in our study. Some consistent trends between the partition coefficients and oxide concentrations were observed and are shown in Figure 4. For example, D_{Ca} and D_{Ti} increase with FeO content of the melt (Figs. 4a and 4b), whereas D_V and D_{Cr} decrease with FeO content of the melt (Figs. 4c and 4d). Because oxide concentrations in the limited number of melt inclusions investigated in this work are not independent of each other, it is not possible to assess whether or not the partition coefficients depend only on FeO. For example, D_{Ca} appears to also decrease with CaO or Al_2O_3 concentration in the melt (Figs. 4e and 4f), which might be an artifact due to the correlation between CaO and FeO and between Al_2O_3 and FeO in the melt.

TABLE 2.—*EXTENDED*

		Na_2O	1σ	K_2O	1σ	Total	Mg#	K_D
74235	OL4					100.4767	71.51734	0.209196
	MI	0.32	0.02	0.060	0.003		34.4	
	WR	0.37–0.4		0.07–0.08				
12040	OL36					98.80222	44.86974	0.375111
	MI	0.36	0.02	0.09	0.01		23.4	
	WR	0.16–1.99		0.04–0.05				
12040	OL41					100.8428	57.39281	0.386647
	MI	0.460	0.004	0.10	0.01		34.2	
	WR	0.16–1.99		0.04–0.05				
12009	OL6					100.7569	73.30917	0.286673
	MI	0.24	0.02	0.05	0.01	96.5	44.1	
	WR	0.23–0.51		0.05–0.06				
12009	OL11					99.95046	73.48023	0.267033
	MI	0.27	0.02	0.06	0.004	98.5	42.5	
	WR	0.23–0.51		0.05–0.06				
15016	OL10					100.9492	70.30001	0.340152
	MI	0.24	0.02	0.03	0.01		44.6	
	WR	0.21–0.32		0.03–0.05				
15647	OL6					99.95885	45.4907	0.294814
	MI	0.24	0.02	0.08	0.01		19.7	
	WR	0.22–0.33		0.04–0.047				

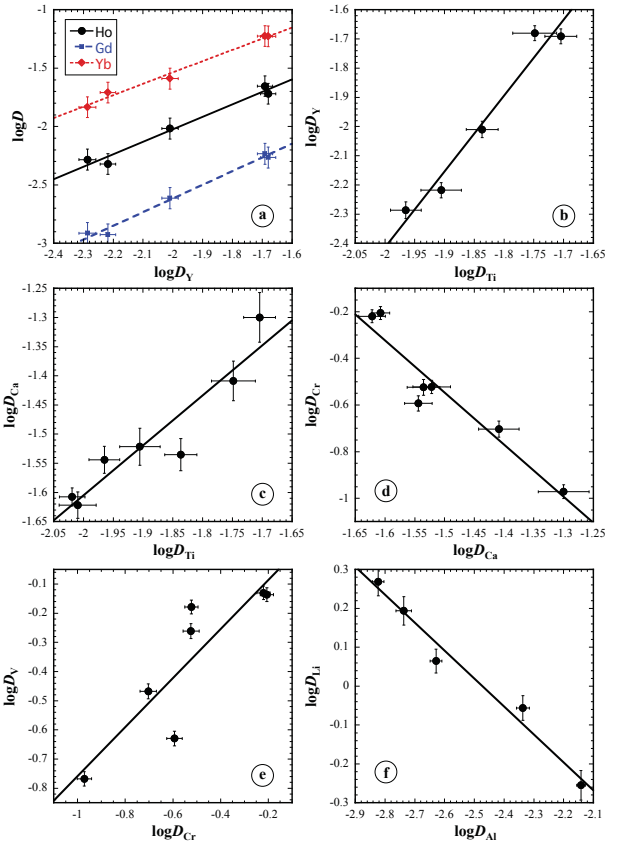

FIGURE 3. Correlations between partition coefficients of selected elements between olivine and melt in lunar basalts. Data are from this study. Error bars are at 1σ level. (Color online.)

TABLE 3. Partition coefficients for major and trace elements between olivine and melt

	74235-OL4	1σ	12040-OL36	1σ	12040-OL41	1σ	12009-OL6	1σ	12009-OL11	1σ	15016-OL10	1σ	15647-OL6	1σ	Literature Min	Literature Max	Ref
Nb	0.0001	0.00003			0.0002	0.00005					0.0008	0.0002	0.0004	0.0001	0.0001	0.0065	[1, 26-27]
Zr	0.0005	0.00004	0.0010	0.0001	0.0004	0.00003					0.0005	0.0000	0.0010	0.0001	0.00015	0.0033	[1, 5, 27]
Gd	0.0012	0.00026	0.0054	0.0011	0.0024	0.00051					0.0012	0.0002	0.0058	0.0012	0.00068	0.033	[10, 13, 26]
Tb	0.0024	0.00049	0.0091	0.0019	0.0052	0.00106					0.0011	0.0002	0.0080	0.0016	0.0011	0.035	[5, 22, 26]
Dy	0.0033	0.00068	0.0134	0.0027	0.0066	0.00136					0.0032	0.0007	0.0125	0.0026	0.014	0.034	[26]
Y	0.0052	0.00034	0.0209	0.0012	0.0098	0.00062					0.0061	0.0004	0.0204	0.0012	0.001	0.045	[1, 5, 10, 13, 22, 26-27]
Ho	0.0052	0.00107	0.0191	0.0039	0.0096	0.00197					0.0048	0.0010	0.0222	0.0045	0.0047	0.037	[10, 22, 26]
Er	0.0073	0.00150	0.0280	0.0057	0.0124	0.00256					0.0095	0.0019	0.0297	0.0060	0.0023	0.045	[1, 5, 26-27]
Tm	0.0116	0.00294	0.0502	0.0127	0.0178	0.00451					0.0193	0.0049	0.0410	0.0104	0.027	0.071	[26]
Yb	0.0146	0.00301	0.0592	0.0120	0.0257	0.00528					0.0196	0.0040	0.0595	0.0121	0.0096	0.071	[1, 4-5, 13, 22, 26-27]
Lu	0.0272	0.00690	0.0753	0.0190	0.0311	0.00788					0.0143	0.0036	0.1062	0.0268	0.0089	0.11	[1, 10-11, 26-27]
Al	0.0072	0.00024	0.0018	0.0001	0.0015	0.00007	0.0045	0.0001	0.0046	0.0002	0.0046	0.0002	0.0024	0.0001	0.0011	0.026	[1-2, 4-8, 10, 12, 15-16, 18-19, 21-22, 28, 29, 31]
Ca	0.0286	0.00153	0.0390	0.0031	0.0292	0.00184	0.0247	0.0009	0.0239	0.0012	0.0301	0.0022	0.0501	0.0049	0.0099	0.078	[1, 3-23, 25, 28, 29-31]
Ti	0.0108	0.00064	0.0178	0.0015	0.0146	0.00090	0.0096	0.0005	0.0098	0.0007	0.0124	0.0010	0.0197	0.0012	0.004	1.01	[4-5, 13-14, 16, 24, 27, 29]
V	0.2347	0.01361	0.3407	0.0203	0.5480	0.03237	0.7307	0.0391	0.7412	0.0396	0.6628	0.0355	0.1707	0.0095	0.003	0.205	[2, 4-5, 13-14, 16, 24, 28]
Li	0.5562	0.04857	1.5624	0.1310	1.8567	0.15696					0.8786	0.0641	1.1604	0.0817	0.29	1.3	[3, 26-27]
Mn	0.6888	0.03857	1.4838	0.0832	1.2382	0.07098	0.9369	0.0497	0.8773	0.0464	0.7199	0.0383	1.0222	0.0556	0.54	3.3	[1, 3-13, 15-17, 19-25, 28, 29]
Cr	0.2550	0.01921	0.1980	0.0158	0.2992	0.02330	0.6228	0.0398	0.6028	0.0385	0.3004	0.0193	0.1068	0.0073	0.39	5.2	[1-7, 14, 16, 24-25, 28, 29]
Fe	1.1400	0.01438	1.7534	0.0358	1.8037	0.01727	1.3839	0.0346	1.3667	0.0344	1.3999	0.0454	1.3412	0.0378	0.48	2.97	[1-23, 25, 28, 29-31]
Co	2.2797	0.1586	3.9780	0.2666	5.0010	0.3385	1.6488	0.0970	1.7823	0.1047	4.0306	0.2377	0.8767	0.0525	1.9	7.34	[4, 13, 16, 22-25]
Mg	5.4496	0.2884	4.6745	0.1189	4.6650	0.2198	4.8275	0.2536	5.1181	0.4019	4.1155	0.4257	4.5492	0.4398	2.3	13	[1-23, 25, 28, 29-31]

References: [1] Salters et al. 2002, [2] Canil 1999, [3] Ottolini et al. 2009, [4] Fellows and Canil 2012, [5] Mallmann and O'Neill 2013, [6] Liu et al. 2014, [7] Righter et al. 2004, [8] Davis and Hirschmann 2013, [9] Brenan et al. 2003, [10] Nielsen et al. 1992, [11] Dunn 1987, [12] Mercer and Johnston 2008, [13] Laubier et al. 2014, [14] Fonseca et al. 2014, [15] Filiberto et al. 2012, [16] Davis et al. 2013, [17] Rosenthal et al. 2015, [18] Koga et al. 2003, [19] Matzen et al. 2013, [20] Liu et al. 2015, [21] Wang and Gaetani 2008, [22] Beattie 1994, [23] Takahashi 1978, [24] Duke 1976, [25] Leeman and Scheidegger 1977, [26] Dunn and Sen 1994, [27] McDade et al. 2003, [28] Canil 1998, [29] Gaetani et al. 2003, [30] Martin et al. 2012, [31] Kinzler et al. 1990

FIGURE 4. Dependence of partition coefficient on major oxide composition in the melt. Black dots are partition data between olivine and melt in lunar basalt from this study. Error bars are at 1σ level.

DISCUSSION

Comparison with literature data

All elemental partition coefficients between olivine and melt obtained for lunar basalts in this study are shown in Table 3, together with minimum and maximum values of partition coefficients for terrestrial basalts. Figure 5 compares partition coefficients in lunar basalts (points with colored symbols) with literature data for terrestrial conditions (gray bars). The literature data for partition coefficients of each element between olivine and mafic melt typically span a large range, 0.7 to 2 orders of magnitude. For most elements, partition coefficients between lunar olivine and basalt determined in this study fall within the range of terrestrial values reported in literature. However, the partition coefficients of Li, V, Cr, Co, Dy, and Tm show differences between our data for lunar basalts and literature data for terrestrial conditions (Fig. 5). The difference in D_{Dy} and D_{Tm} between lunar and terrestrial basalts is likely due to the lack of experimental data: only one paper reported experimental Dy and Tm partition data for terrestrial conditions. For example, if interpolated D_{Dy} and D_{Tm} in Nielsen et al. (1992) (as listed in Geochemical Earth Reference Model website, https://earthref.org/KDD/) were included, the terrestrial range would cover all the lunar Dy and Tm data. For Co, one lunar sample (15647) has a lower Co partition coefficient than in other lunar samples and in literature terrestrial data. The calibration curve for

Co in olivine has more scatter than for other elements (Zn, Cu, and Ni calibration curves show even more scatter and are deemed unsatisfactory and were not used). Hence, we will not emphasize the single point. Below, we examine the differences in D_{Li}, D_{Cr}, and D_V between lunar and terrestrial basalts.

The partition coefficient of Li between olivine and basalt is higher in some lunar samples than in terrestrial samples. D_{Li} appears to increase with the Fa# [=Fe/(Fe+Mg) of olivine] (Fig. 6a). Literature D_{Li} data are limited (Dunn and Sen 1994; Brenan et al. 1998; Taura et al. 1998; McDade et al. 2003; Ottolini et al. 2009; Dalou et al. 2012; Nielsen and Ustunisik 2019). Only 25 data points satisfy the following conditions: nominally dry, <20% relative error on Li concentrations, containing >30 wt% SiO_2, and having both olivine and melt composition reported. All these literature data values are for low-Fa# olivine (Fa# ≤ 0.22 or Fo# ≥ 0.78), whereas D_{Li} values in this work are for samples with Fa# as high as 0.55, leading to higher D_{Li} values in the Fe-rich samples (Fig. 6a). One explanation for the increase of D_{Li} with Fa# is that the ionic radius of Li^+ (0.76 Å in octahedral site, Shannon 1976) is more similar to that of high-spin Fe^{2+} (0.78 Å) than to Mg^{2+} (0.72 Å). We modeled the dependence of D_{Li} on temperature, pressure, and composition and determined that the pressure effect is insignificant. A rough fit is as follows:

$$\ln D_{Li} = 3.33 + [-13457 + 8216\sqrt{Fa\#} + 51.9(SiO_2 + 2Al_2O_3)]/T \quad (1)$$

where T is in Kelvin, and SiO_2 and Al_2O_3 are in wt% in the melt (i.e., 50 wt% SiO_2 means SiO_2 = 50 in the above equation, not 0.5). The above equation can reproduce $\ln D_{Li}$ data with a standard deviation of 0.19 after excluding two outlier points (Fig. 6b). Based on the above equation, D_{Li} between olivine and melt increases with Fa# in olivine and $SiO_2 + 2Al_2O_3$ in the melt.

Chromium exists mainly in the form of Cr^{3+} in terrestrial basalts, but a significant fraction of Cr is Cr^{2+} under the reducing conditions in lunar glass and minerals (Schreiber and Haskin 1976; Sutton et al. 1993; Papike et al. 2005; Berry et al. 2006; Bell et al. 2014; Simon and Sutton 2017). Considerable research has been devoted to Cr partitioning under terrestrial and lunar conditions, showing complicated Cr partitioning behavior between olivine and melt. Schreiber and Haskin (1976) determined Cr partition coefficients in forsterite-anorthite-diopside and forsterite-anorthite-silica systems with an f_{O_2} range of about 10 orders of magnitude and showed that D_{Cr} between forsterite and melt depends on temperature, composition, and f_{O_2}. D_{Cr} data by Mikouchi et al. (1994) and Gaetani and Grove (1997) in FeO-bearing systems and a narrower f_{O_2} range showed no dependence on f_{O_2}. Hanson and Jones (1998) reconciled these results by proposing that Cr^{3+} partitioning was sensitive to composition, whereas Cr^{2+} partitioning was highly sensitive to temperature. Consequently, for a certain composition and temperature, the Cr^{3+} partition coefficient is similar to that of Cr^{2+}, leading to approximately constant D_{Cr} with f_{O_2}. Mallmann and O'Neill (2009) reported that for some melts that contain <1.7 wt% FeO at 1300 °C, the Cr partition coefficient between olivine and melt is roughly constant between QFM-10 and QFM+4. Yet, our data show that the Cr partition coefficient between olivine and melt in lunar basalts is significantly lower than that in terrestrial rocks. The significantly lower D_{Cr} in lunar basalts than in terrestrial basalts must be due to differences in some combination of composition, f_{O_2}, and temperature (Hanson and Jones 1998).

We modeled D_{Cr} as a function of temperature, olivine and melt composition, and f_{O_2}. The following criteria were used in filtering literature D_{Cr} data: (1) f_{O_2} values must be reported for each D_{Cr} value; (2) if Cr_2O_3 concentration is measured by electron microprobe, the Cr_2O_3 concentration must be >0.10 wt% so that it does not have too large an uncertainty; (3) the 1σ uncertainty must be <20% of the measured concentration; and (4) the chemical composition must contain <5 wt% other oxides in addition to the typical major oxides. Data sources are listed in Figure 7.

We first tried using an empirical linear model in which $\ln D_{Cr}$ is assumed to be linearly dependent on $1000/T$, P, $\log f_{O_2}$, $(1 - Fo\#_{oliv})^2/T$, X_i/T (where X_i is the cation mole fraction of Si, Ti, Al, etc.), plus various multiplications of these terms. The model is similar to but includes more complicated terms than the model of Mallmann and O'Neill (2013) for V partitioning. Unfortunately, this effort did not lead to satisfactory fits (e.g., mean error in reproducing $\ln D_{Cr}$ being ≤0.2) even with ≥14 parameters unless some coefficients were large positive and negative values, leading to wide swings in the calculated $\ln D_{Cr}$, which are indicative of overfitting.

We then tried to model D_{Cr} as a function of temperature, pressure, melt composition, and f_{O_2} using a quasi-thermodynamically based formulation. In this formulation, D_{Cr} is related to D_{CrO}, $D_{CrO1.5}$ (CrO_3 is not included for simplicity), and the equilibrium constant K_{hom} for the homogeneous reaction of CrO(melt) + (1/4) $O_2 \rightleftharpoons CrO_{1.5}$(melt) as follows (e.g., Mallmann and O'Neill 2009):

$$\ln D_{Cr} = \ln \frac{D_{Cro} + D_{Cro_{1.5}} K_{hom} f_{O_2}^{1/4}}{1 + K_{hom} f_{O_2}^{1/4}}. \quad (2)$$

Each of $\ln D_{CrO}$, $\ln D_{CrO1.5}$, and $\ln K_{hom}$ is expressed as a linear function of $1/T$, P/T, Fo#/T, X_i/T in the melt, and X_iX_j/T (e.g.,

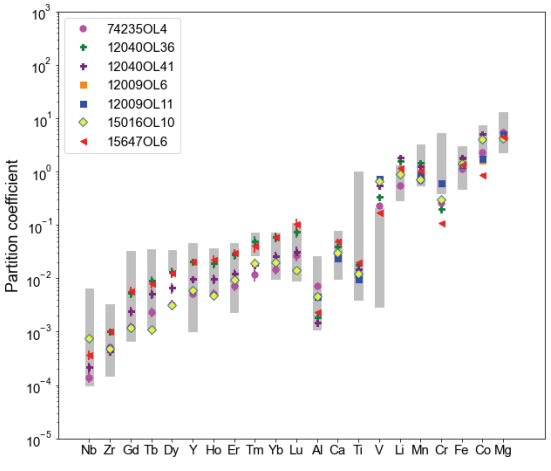

FIGURE 5. Partition coefficients between olivine and melt in lunar basalt from this study (colored symbols) compared with literature data at terrestrial conditions (gray vertical bars). Data and references can be found in Table 3. The partition coefficients for terrestrial basalts are selected from literature data based on the following criteria: experimental data only, $\log f_{O_2}$ greater than QFM-2, and melt compositions with 2 to 20 wt% FeO_t, >10 wt% Al_2O_3, and < 5 wt% TiO_2. (Color online.)

regular solution model would have X_iX_j/T terms in the activity coefficients). Such a model requires nonlinear minimization involving numerous terms, which was performed using MatLab. The terms are added or removed based on the examination of fitting results. However, by increasing the number of fitting parameters to improve fitting precision, some fitting parameters would assume large positive and negative values, leading to wide swings in the calculated D_{Cr} values. After much effort, we decided to adopt the following less complicated model to avoid overfitting:

$$\ln D_{CrO} = -2.92 + 41\,698 \cdot Si \cdot Mg/T \quad (3a)$$
$$\ln D_{CrO1.5} = -4.52 + [5395 + 1338Fo\# + 35\,299(Na + K)]/T \quad (3b)$$
$$\ln K_{hom} = -79.00 + [104\,330 + 126\,061(Mg + Ca + Na + K)]/T \quad (3c)$$

where T is temperature in kelvin, Si, Mg, Ca, Na, and K are cation mole fractions of the melt, and Fo# = Mg/(Mg+Fe) in olivine.

Using D_{CrO}, $D_{CrO1.5}$, and K_{hom} in Equations 3a, 3b, and 3c to calculate $\ln D_{Cr}$ in Equation 2, experimental $\ln D_{Cr}$ values can be reproduced with a standard deviation of 0.20 ln$D$ units (Fig. 7) after excluding 15 points. However, K_{hom} values based on the fitting results parameters vary by 11 orders of magnitude over the temperature and composition range of the literature data, which may be unrealistic. Hence, even though $\ln D_{Cr}$ values can be roughly reproduced using the fit, the physical interpretation of the fitted D_{CrO}, $D_{CrO1.5}$, and especially K_{hom} may not be meaningful. Based on Equations 3a to 3c, the lower D_{Cr} values between olivine and melt in lunar basalts may be attributed to lower Fo#, lower Si·Mg, and lower Mg(Na+K) than terrestrial basalts. Hence, key experimental data to improve understanding and modeling of Cr partition between olivine and melt appear to be those with lower Fo# (down to at least 0.5, which also means low-MgO concentration in the melt) and at a large range of f_{O_2}.

In addition to the above quasi-thermodynamically based modeling, we also examined different substitution mechanisms to explain the variation of the Cr partition coefficient but did not arrive at satisfactory answers.

Vanadium partitioning has been evaluated systematically in numerous studies and has been found to be insensitive to temperature or composition but to increase strongly with decreasing f_{O_2} (e.g., Canil 1997; Mallmann and O'Neill 2009, 2013; Papike et al. 2013). Therefore, the partitioning of V has been used as an important redox indicator (e.g., Canil and Fedortchouk 2001; Shearer et al. 2006; Wood et al. 2008; Mallmann and O'Neill 2013). The V partition coefficient data for lunar samples range from 0.17 to 0.74, with an average of ~0.43, and are systematically higher than the values of 0.003 to 0.21 reported for terrestrial basalts (Table 3). This result is expected because lunar basalts are much more reduced than terrestrial basalts. For example, XANES measurements of lunar samples show that V in lunar basalts is predominantly in the form of V^{3+}, with up to 20% of V^{2+} (Sutton et al.

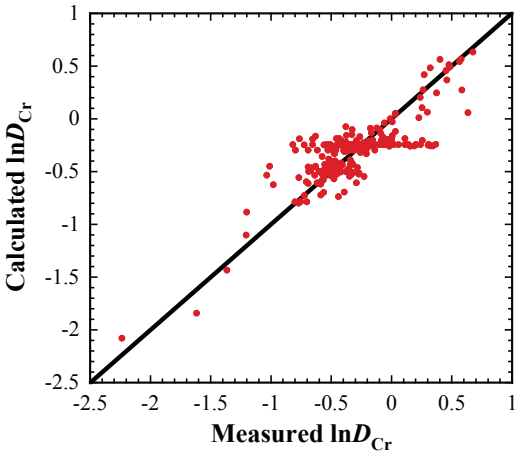

FIGURE 7. Fit of Cr partition coefficient data using equation 2 with parameters given in Equations 3a to 3c. Literature Cr partition data are from EarthChem (Nielsen and Ustunisik 2019), Beattie (1994), Canil (1998, 1999), Hanson and Jones (1998), Righter et al. (2004), Mallmann and O'Neill (2009, 2013), Tuff and O'Neill (2010), Fellows and Canil (2012), Davis et al. (2013), Bell et al. (2014), Fonseca et al. (2014), Liu et al. (2014), and Leitzke et al. (2016). Fifteen data points are excluded, including 7 points in Mallmann and O'Neill (2009), 3 in Fonseca et al. (2014), 3 in Leitzke et al. (2016), and 2 points in Liu et al. (2014). (Color online.)

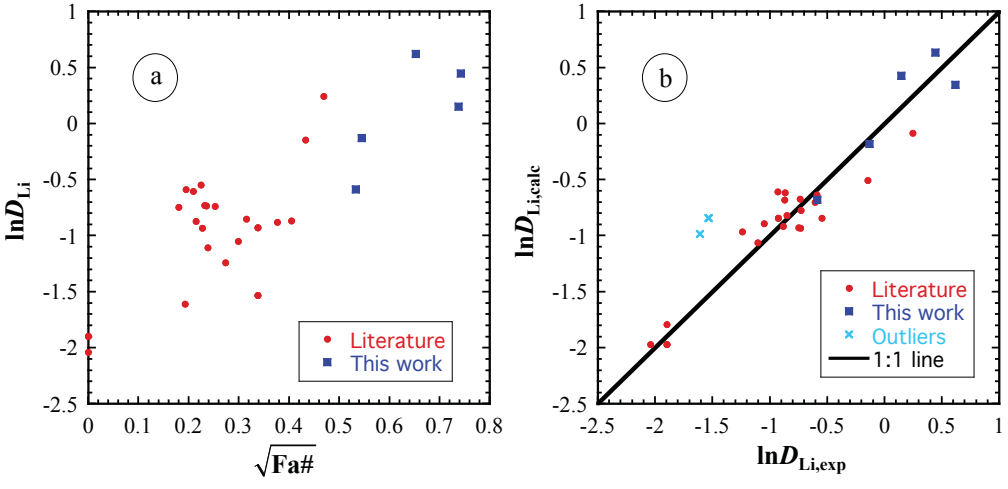

FIGURE 6. (**a**) Correlation between $\ln D_{Li}$ and square root of Fa# in olivine. (**b**) Comparison of calculated $\ln D_{Li}$ using Equation 1 (vertical axis) with experimental values (horizontal axis). Data sources include: Dunn and Sen (1994); Brenan et al. (1998); Taura et al. (1998); McDade et al. (2003); Ottolini et al. (2009); Dalou et al. (2012); Nielsen and Ustunisik (2019). Data with >20% relative error in Li concentration or with <10 wt% SiO_2 are excluded. Two outlier points are from Taura et al. (1998) and Dalou et al. (2012). (Color online.)

2005; Karner et al. 2006). The dominant valence state in terrestrial basalts, however, is V^{4+} (Papike et al. 2005), which explains the difference in V partition coefficients between lunar and terrestrial samples. The observed variation of V partition coefficient from 0.17 to 0.74 in lunar basalts can be explained by variations of $\log f_{O_2}$, from NNO-3.17 to NNO-5.86 (IW+1.5 to IW-1.2) according to the relationship between D_V and $\log f_{O_2}$ of Canil (1997), or from IW+1.5 to IW-1.8 using the model of Mallmann and O'Neill (2009), which are roughly consistent with the estimated oxygen fugacity for lunar basalts [IW-2 to IW, (Sato et al. 1973; Wadhwa 2008)]. There may also be significant dependence of V partition coefficient on melt composition, as recently modeled empirically by Mallmann and O'Neill (2013). However, although the model by Mallmann and O'Neill (2013) attempted to improve the model of Mallmann and O'Neill (2009) by incorporating the compositional dependence of D_V, it fails to reproduce the measured D_V values in this study by assuming a reasonable f_{O_2} for lunar basalts (from IW to IW-2): the predicted D_V values would be too high by up to 1.5 orders of magnitude. This points to the limitations of empirical modeling of the partition coefficient of V, which has multiple oxidation states. Due to the difficulty in our modeling of Cr partition coefficient, and because there are more potential oxidation states for V, we did not attempt to model V partition coefficient using a thermodynamically based formulation. Nonetheless, our data on V partitioning are as expected.

Implications

The olivine-melt partition coefficients for lunar mare basalts obtained in this study may be applied to investigate the effect of olivine fractionation during lunar basaltic magma evolution and shallow-level (low-pressure) lunar magma ocean evolution. In addition, our data for olivine-melt partitioning can be combined with partition data between other mantle minerals and melt to quantify trace element behavior during lunar mantle partial melting and trace element concentration in primary mare basalts and the lunar mantle.

Data for most elements in this study for lunar olivine-melt partitioning are similar to those for terrestrial basalts. Hence, no reconsideration is needed for relevant modeling for those elements. However, Li, V, and Cr partition coefficients between olivine and melt in lunar basalts are significantly different from those in terrestrial basalts. There are several consequences of this.

As shown in Figure 6a, Li becomes a compatible element in olivine when the Fa# in olivine is >0.25, which roughly corresponds with a low Mg# ≤ 0.47 in the melt using a K_D value of 0.3. That is, in evolved basalt, Li is compatible in olivine relative to melt. However, because the Li partition coefficient in pyroxenes is smaller than that in olivine (Ottolini et al. 2009), the effect of the increased compatibility of Li in olivine in evolved basalt does not appear to result in a clear shift in Li behavior when lunar basalts and terrestrial basalts are compared. Hence, it does not seem that the slightly different Li partition coefficient results in significantly different behavior between lunar basalts and terrestrial basalts.

The Cr partition coefficient between olivine and melt is smaller in lunar basalts than in terrestrial basalts. Combined with the observation that Cr partition coefficient between clinopyroxene and melt and between orthopyroxene and melt decreases with decreasing f_{O_2} (Canil 1999; Mallmann and O'Neill 2009), Cr is an incompatible element during lunar mantle partial melting and early basalt evolution, which is opposite to it being strongly compatible during terrestrial mantle partial melting and basalt evolution. Therefore, Cr concentration in mantle-derived basalts is expected to be high, and to become higher in evolved melts before oxide minerals crystallize. That is, the higher Cr concentration in lunar olivine than in terrestrial olivine (e.g., Steele and Smith 1975) is not due to a larger Cr partition coefficient but to a higher Cr concentration in the melt (Schreiber and Haskin 1976).

Figure 8 displays Cr vs. MgO and Cr vs. FeO in terrestrial and lunar basalts. MgO is a compatible oxide and lower MgO concentration typically means more evolved basalts. Cr concentrations in lunar basalts are much higher than in terrestrial MORB and OIB, as expected from its incompatibility in the lunar mantle and its compatibility in the terrestrial mantle. Furthermore, in terrestrial MORB and OIB, Cr shows a relatively simple positive (roughly linearly) correlation with MgO, indicating that Cr is a compatible element similar to MgO during terrestrial basalt evolution. On the other hand, the Cr vs. MgO trend in lunar basalts is more complicated: Cr concentration increases with decreasing MgO from 25 to ~11 wt%, and then decreases with further decreasing MgO. Hence, Cr is incompatible when MgO concentration is above 11 wt% (primitive basalt) but becomes compatible when MgO concentration is below 11 wt%. The trend of first increasing and then decreasing Cr concentration as MgO decreases in lunar basalts are similar to the FeO vs. MgO trend in terrestrial basalts (Grove and Baker 1984) and might be controlled by the crystallization of chromite and/or other oxide minerals. In Cr vs. FeO (Fig. 8b), Cr is crudely positively correlated with FeO in lunar basalts (Seifert and Ringwood 1988), with Cr being more incompatible than FeO, indicating that Cr and Fe are both incompatible during mafic silicate mineral fractionation and compatible in Fe-Ti oxides. On the other hand, in terrestrial basalts, Cr concentration has a maximum at approximately 9 wt% FeO in MORB and 12 wt% FeO in OIB because starting from the maximum Cr concentration, tholeiitic FeO enrichment is accompanied by Cr depletion (Cr is compatible), and subsequent FeO depletion due to oxide crystallization is also accompanied by Cr depletion.

Vanadium partition coefficient between olivine and melt is higher in lunar settings than in terrestrial settings because of the more reduced lunar conditions. Combined with increasing V partition coefficients between other mafic minerals and melt as f_{O_2} decreases (Mallmann and O'Neill 2009), V is expected to be less incompatible during lunar basalt evolution than in terrestrial basalt evolution. Figure 9 confirms this expectation. In terrestrial basalts, V is highly incompatible in primitive basalts, whereas Mg is compatible. Hence, V concentration increases steeply as MgO concentration decreases (Fig. 9a, MORB and OIB trends). At lunar conditions, however, V is incompatible when MgO is greater than approximately 11 wt% (meaning that V concentration increases as MgO concentration decreases), but less so than in terrestrial basalts. At lower MgO, V in lunar basalts becomes compatible and decreases as MgO decreases. Vanadium concentration in lunar basalts when plotted against MgO also has a maximum at ~10 to 12 wt% MgO, which is similar to Cr. The positive trends of V-FeO_t for both terrestrial and lunar samples but with a lower slope for lunar samples also indicate that V in terrestrial basalts is much more incompatible than in lunar basalts.

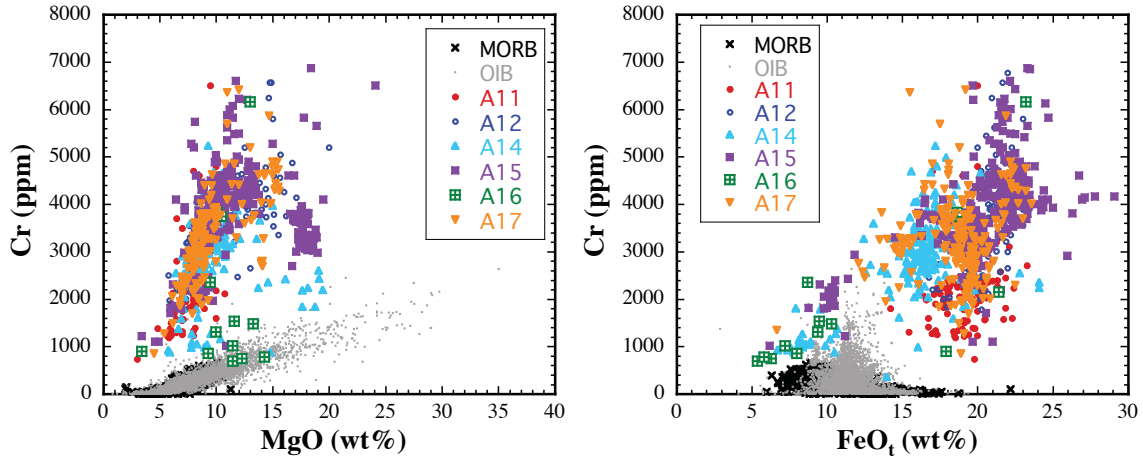

Figure 8. Cr concentration vs. MgO and Cr vs. FeO_t in lunar basalts and terrestrial MORB and OIB ($SiO_2 \leq 55$ wt%). Lunar basalt data are from Mare Basalt Database (https://www3.nd.edu/~cneal/lunar-l/), MORB data are from the compilation by Gale et al. (2013) and OIB data are from GeoRoc. (Color online.)

The partition coefficients of V and Cr between olivine and melt are similar in lunar basalts (0.17 to 0.74 for V vs. 0.11 to 0.62 for Cr). However, in terrestrial basalts, the partition coefficient for V is much smaller than that of Cr. Hence, olivine fractionation would not significantly change the V/Cr ratio in the lunar magma ocean or lunar basalts, but V/Cr ratio in terrestrial basalts would increase significantly with olivine fractionation. The similarity of V and Cr partition coefficients between olivine and melt in lunar basalts apparently also applies to other mafic minerals in lunar settings, which leads to a nearly constant V/Cr ratio in lunar basalts (Seifert and Ringwood 1988). Figure 10 shows V vs. Cr concentrations in lunar basalts and terrestrial MORB and OIB, and indicates that V and Cr are positively correlated in lunar basalts (Fig. 10a) with a nearly constant V/Cr ratio. Because some authors argue that the constancy of an elemental ratio is best examined by using a log-log concentration plot (Sims and DePaolo 1997; Hofmann et al. 2020), we do so in Figure 10b. A slope of 1 in the log-log plot means a constant V/Cr ratio. In Figure 10b, even though there is much scatter (most of the very low V/Cr ratios are from A11 samples, and most of the high V/Cr ratios are from A17 samples), the slope from the simple linear fitting of log(V) vs. log(Cr) is 0.956 ± 0.037 (1σ error), which is ~1. After removing the outliers (outside 3σ), the average V/Cr slope in lunar basalts is 0.039 ± 0.011, which is in excellent agreement with the ratio of 0.038 obtained by Seifert and Ringwood (1988). The V/Cr ratio in lunar basalts is not much different from the ratio in the bulk silicate Earth (0.031; McDonough and Sun 1995). The depletion of Cr (50% condensation temperature is 1296 K by Lodders 2003; 1291 K by Wood et al. 2019) in the Moon relative to V (condensation temperature is 1429 K by Lodders 2003; 1370 K by Wood et al. 2019) is small, about 20% based on the ratios, which is within the errors of the V/Cr ratios.

Because the data in Figure 10 reflect the involvement of not only olivine but also other minerals, Figure 10 shows that V and Cr have similar degrees of incompatibility not only in olivine, as shown in this study, but also in other minerals in lunar basalts. Because element pairs with nearly constant ratios are often used to estimate the mantle composition (e.g., McDonough and Sun 1995; Salters and Stracke 2004; Hofmann et al. 2020) as well as particular processes that might affect a given ratio (e.g., Cooper

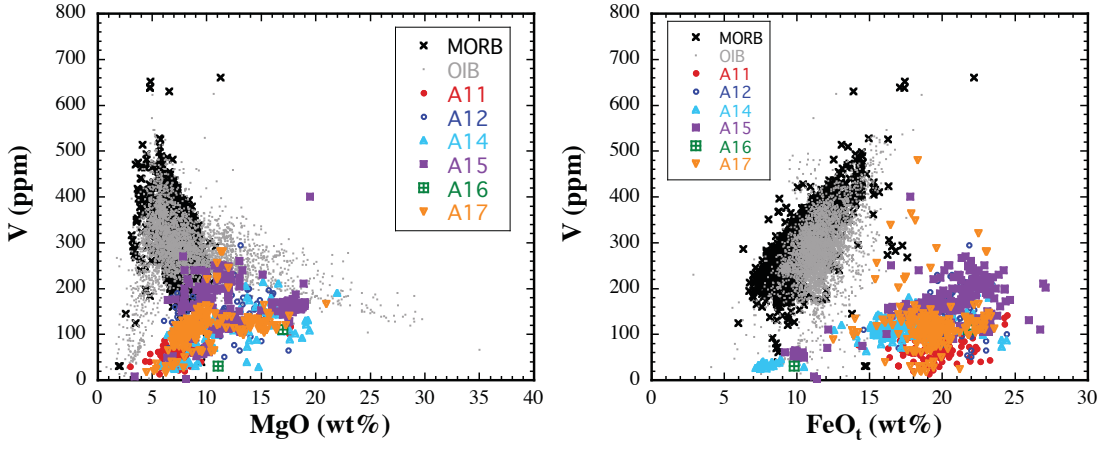

Figure 9. Vanadium concentration vs. MgO and FeO in lunar and terrestrial basalts. Data sources are the same as Figure 8. (Color online.)

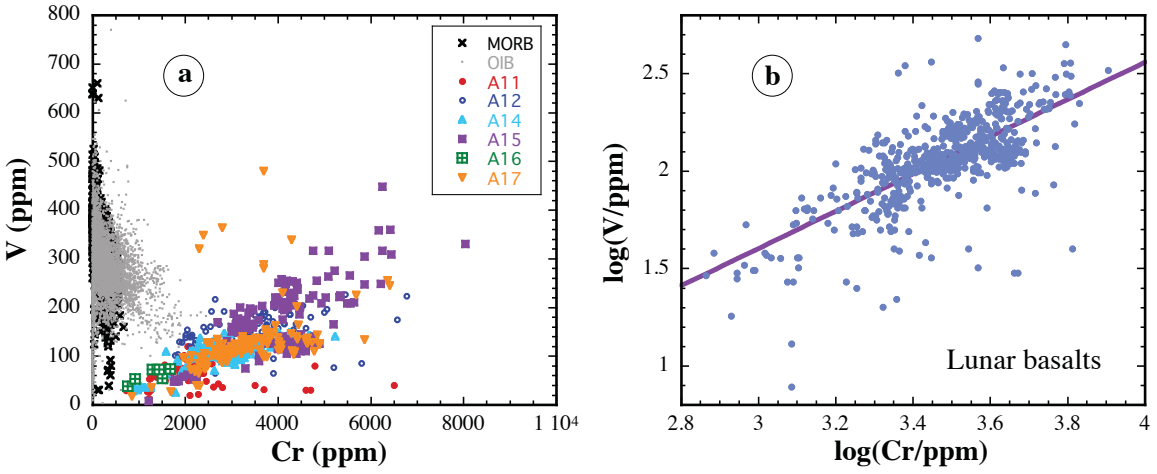

Figure 10. Vanadium concentration vs. Cr concentration in lunar and terrestrial basalts. Data sources are the same as Figure 8. (Color online.)

et al. 2012), the similar degree of incompatibility for V and Cr provides a useful tool for examining lunar basalt evolution, as well as the lunar mantle composition.

To conclude, partition coefficients between olivine and melt in lunar basalts are measured for 21 elements. Most of our new data are in good agreement with those in terrestrial basalts despite the large differences in basalt composition and oxygen fugacity, except for the partition coefficients of Li, V, and Cr. The slightly higher Li partition coefficient between olivine and melt in lunar basalts than in terrestrial basalts is largely due to the higher Fa# in olivine in typical lunar basalts and does not seem to lead to clear and consistent consequences in Li behavior during lunar basalt evolution. The higher V partition coefficients in lunar basalts can be readily explained by the lower oxidation state of lunar basalts compared to terrestrial basalts. On the other hand, the smaller partition coefficients of Cr in lunar basalts than in terrestrial basalts seem to be due to compositional effects. Chromium behaves as an incompatible element during crystal fractionation of lunar basalt when MgO is ≥11 wt%, which is opposite to its compatibility during terrestrial basalt evolution. Vanadium is less incompatible during lunar basalt evolution than terrestrial basalt evolution. In addition, V and Cr have similar partition coefficients between mafic minerals and basalt in the Moon, confirming the results by Seifert and Ringwood (1988). Our new partition data can also explain: (1) the much higher Cr concentration in high-FeO lunar basalts than in terrestrial basalts; (2) the much lower V concentration in evolved lunar basalts than in evolved terrestrial basalts; and (3) the roughly constant V/Cr ratio of ~0.039 in lunar basalts (Seifert and Ringwood 1988). The partition coefficients determined in this study can be applied to model lunar magma evolution, to infer melt composition from olivine composition, and to model partial melting of the lunar mantle.

Acknowledgments and Funding

We thank Dante Danil and an anonymous reviewer for their constructive reviews, which significantly improved this paper. This work was supported by NASA grant NNX15AH37G and 80NSSC19K0782, and NSF grants EAR-1829822 and EAR-2020603. We thank NASA CAPTEM for providing the lunar samples, K.P. Jochum for providing the MPI-DING glass standards, J.C. Barrette for assistance in LA-ICP-MS analyses, and Yunbin Guan for assistance in SIMS analyses. The electron microprobe Cameca SX100 used in this study was purchased using NSF grant EAR-9911352.

References cited

Beattie, P. (1994) Systematics and energetics of trace-element partitioning between olivine and silicate melts: Implications for the nature of mineral/melt partitioning. Chemical Geology, 117, 57–71.

Bell, A.S., Burger, P.V., Le, L., Shearer, C.K., Papike, J.J., Sutton, S.R., Newville, M., and Jones, J. (2014) XANES measurements of Cr valence in olivine and their applications to planetary basalts. American Mineralogist, 99, 1404–1412.

Berry, A.J., O'Neill, H.St.C., Scott, D.R., Foran, G.J., and Shelley, J.M.G. (2006) The effect of composition on Cr^{2+}/Cr^{3+} in silicate melts. American Mineralogist, 91, 1901–1908.

Borisov, A., Lahaye, Y., and Palme, H. (2004) The effect of TiO_2 on Pd, Ni, and Fe solubilities in silicate melts. American Mineralogist, 89, 564–571.

Brenan, J.M., Neroda, E., Lundstrom, C.C., Shaw, H.F., Ryerson, F.J., and Phinney, D.L. (1998) Behavior of boron, beryllium, and lithium during melting and crystallization: Constraints from mineral-melt partitioning experiments. Geochimica et Cosmochimica Acta, 62, 2129–2141.

Brenan, J.M., McDonough, W.F., and Dalpé, C. (2003) Experimental constraints on the partitioning of rhenium and some platinum-group elements between olivine and silicate melt. Earth and Planetary Science Letters, 212, 135–150.

Canil, D. (1997) Vanadium partitioning and the oxidation state of Archaean komatiite magmas. Nature, 389, 842–845.

——— (1998) Vanadium partitioning and the oxidation state of Archaean komatite magmas. Nature, 389, 842–845. doi: 10.1038/39860

——— (1999) Vanadium partitioning between orthopyroxene, spinel and silicate melt and the redox states of mantle source regions for primary magmas. Geochimica et Cosmochimica Acta, 63, 557–572.

Canil, D., and Fedortchouk, Y. (2001) Olivine-liquid partitioning of vanadium and other trace elements, with applications to modern and ancient picrites. Canadian Mineralogist, 39, 319–330.

Charlier, B., Grove, T.L., Namur, O., and Holtz, F. (2018) Crystallization of the lunar magma ocean and the primordial mantle-crust differentiation of the Moon. Geochimica et Cosmochimica Acta, 234, 50–69.

Chen, Y., and Zhang, Y. (2008) Olivine dissolution in basaltic melt. Geochimica et Cosmochimica Acta, 72, 4756–4777.

——— (2009) Clinopyroxene dissolution in basaltic melt. Geochimica et Cosmochimica Acta, 73, 5730–5747.

Chen, Y., Provost, A., Schiano, P., and Cluzel, N. (2013) Magma ascent rate and initial water concentration inferred from diffusive water loss from olivine-hosted melt inclusions. Contributions to Mineralogy and Petrology, 165, 525–541.

Chen, Y., Zhang, Y., Liu, Y., Guan, Y., Eiler, J., and Stolper, E.M. (2015) Water, fluorine, and sulfur concentrations in the lunar mantle. Earth and Planetary Science Letters, 427, 37–46.

Cooper, L.B., Ruscitto, D.M., Plank, T., Wallace, P.J., Syracuse, E.M., and Manning, C.E. (2012) Global variations in H_2O/Ce: 1. Slab surface temperatures beneath volcanic arcs. Geochemistry, Geophysics, Geosystems, 13, Q03024.

Davis, F.A., and Hirschmann, M.M. (2013) The effects of K_2O on the compositions of near-solidus melts of garnet peridotite at 3 GPa and the origin of basalts from enriched mantle. Contributions to Mineralogy and Petrology, 166, 1029–1046.

Davis, F.A., Humayun, M., Hirschmann, M.M., and Cooper, R.S. (2013) Experimentally determined mineral/melt partitioning of first-row transition elements (FRTE) during partial melting of peridotite at 3 GPa. Geochimica et Cosmochimica Acta, 104, 232–260.

Dalou, C., Koga, K.T., Shimizu, N., Boulon, J., and Devidal, J.L. (2012) Experimental

determination of F and Cl partitioning between lherzolite and basaltic melt. Contributions to Mineralogy and Petrology, 163, 591–609.
Donaldson, C.H., Usselman, T.M., Williams, R.J., and Lofgren, G.E. (1975) Experimental modeling of the cooling history of Apollo 12 olivine basalts. 6th Lunar Science Conference, 843–869.
Duke, J.M. (1976) Distribution of the period four transition elements among olivine, calcic clinopyroxene and mafic silicate liquid: Experimental results. Journal of Petrology, 17, 499–521.
Dunn, T. (1987) Partitioning of Hf, Lu, Ti, and Mn between olivine, clinopyroxene and basaltic liquid. Contributions to Mineralogy and Petrology, 96, 476–484.
Dunn, T., and Sen, C. (1994) Mineral/matrix partition coefficients for orthopyroxene, plagioclase, and olivine in basaltic to andesitic systems: A combined analytical and experimental study. Geochimica et Cosmochimica Acta, 58, 717–733.
Dygert, N., Liang, Y., and Hess, P. (2013) The importance of melt TiO_2 in affecting major and trace element partitioning between Fe–Ti oxides and lunar picritic glass melts. Geochimica et Cosmochimica Acta, 106, 134–151.
Elardo, S.M., Draper, D.S., and Shearer, C.K. (2011) Lunar Magma Ocean crystallization revisited: Bulk composition, early cumulate mineralogy, and the source regions of the highlands Mg-suite. Geochimica et Cosmochimica Acta, 75, 3024–3045.
Fellows, S.A., and Canil, D. (2012) Experimental study of the partitioning of Cu during partial melting of Earth's mantle. Earth and Planetary Science Letters, 337-338, 133–143.
Filiberto, J., Wood, J., Dasgupta, R., Shimizu, N., Le, L., and Treiman, A.H. (2012) Effect of fluorine on near-liquidus phase equilibria of an Fe–Mg rich basalt. Chemical Geology, 312-313, 118–126.
Fonseca, R.O.C., Mallmann, G., Sprung, P., Sommer, J.E., Heuser, A., Speelmanns, I.M., and Blanchard, H. (2014) Redox controls on tungsten and uranium crystal/silicate melt partitioning and implications for the U/W and Th/W ratio of the lunar mantle. Earth and Planetary Science Letters, 404, 1–13.
Gaetani, G.A., and Grove, T.L. (1997) Partitioning of moderately siderophile elements among olivine, silicate melt, and sulfide melts: Constraints on core formation in the Earth and Mars. Geochimica et Cosmochimica Acta, 61, 1829–1846.
Gaetani, G.A., and Watson, E.B. (2000) Open system behavior of olivine-hosted melt inclusions. Earth and Planetary Science Letters, 183, 27–41.
——— (2002) Modeling the major-element evolution of olivine-hosted melt inclusions. Chemical Geology, 183, 25–41.
Gaetani, G.A., Kent, A.J.R., Grove, T.L., Hutcheon, I.D., and Stolper, E.M. (2003) Mineral/melt partitioning of trace elements during hydrous peridotite partial melting. Contributions to Mineralogy and Petrology, 145, 391–405. doi: 10.1007/s00410-003-0447-0
Gale, A., Dalton, C.A., Langmuir, C.H., Su, Y., and Schilling, J.-G. (2013) The mean composition of ocean ridge basalts. Geochemistry, Geophysics, Geosystems, 14, 489–518.
Grove, T.L., and Baker, M.B. (1984) Phase equilibrium controls on the tholeiitic versus calc-alkaline differentiation trends. Journal of Geophysical Research: Solid Earth, 89, 3253–3274.
Hanson, B., and Jones, J.H. (1998) The systematics of Cr^{3+} and Cr^{2+} partitioning between olivine and liquid in the presence of spinel. American Mineralogist, 83, 669–684.
Hauri, E.H., Weinreich, T., Saal, A.E., Rutherford, M.J., and Van Orman, J.A. (2011) High pre-eruptive water contents preserved in lunar melt inclusions. Science, 333, 213–215.
Hofmann, A.W., Class, C., and Goldstein, S.L. (2020) Size and composition of the residual and depleted mantle reservoir. Preprint, doi: 10.1002/essoar.10501102.1.
Jochum, K.P., Nohl, U., Herwig, K., Lammel, E., Stoll, B., and Hofmann, A.W. (2005) GeoRem: A new geochemical database for reference materials and isotopic standards. Geostandards and Geoanalytical Research, 29, 333–338.
Jochum, K.P., Stoll, B., Herwig, K., Willbold, M., Hofmann, A.W., Amini, M., Aarburg, S., Abouchami, W., Hellebrand, E., Mocek, B., and others (2006) MPI-DING reference glasses for in situ microanalysis: new reference values for element concentrations and isotope ratios. Geochemistry, Geophysics, Geosystems, 7(2), Q02008, doi: 10.1029/2005GC001060.
Jochum, K.P., Weis, U., Stoll, B., Kuzmin, D., Yang, Q., Raczek, I., Jacob, D.E., Stracke, A., Birbaum, K., Frick, D.A., Gunther, D., and Enzweiler, J. (2011) Determination of reference values for NIST SRM 610-617 glasses following ISO guidelines. Geostandards and Geoanalytical Research, 35, 397–429.
Karner, J.M., Sutton, S.R., Papike, J.J., Shearer, C.K., Jones, J.H., and Newville, M. (2006) Application of a new vanadium valence oxybarometer to basaltic glasses from the Earth, Moon, and Mars. American Mineralogist, 91, 270–277.
Kinzler, R.J., Grove, T.L., and Recca, S.I. (1990) An experimental study on the effect of temperature and melt composition on the partitioning of nickel between olivine and silicate melt. Geochimica et Cosmochimica Acta, 54(5), 1255–1265. doi: 10.1016/0016-7037(90)90151-A
Koga, K., Hauri, E., Hirschmann, M., and Bell, D. (2003) Hydrogen concentration analyses using SIMS and FTIR: Comparison and calibration for nominally anhydrous minerals. Geochemistry, Geophysics, Geosystems, 4.
Langmuir, C.H., Hanson, G.N., O'Hara, M.J., Bailey, D.K., Tarney, J., and Dunham, K.C. (1980) An evaluation of major element heterogeneity in the mantle sources of basalts. Philosophical Transactions of the Royal Society of London. Series A, Mathematical and Physical Sciences, 297, 383–407.
Laubier, M., Grove, T.L., and Langmuir, C.H. (2014) Trace element mineral/melt partitioning for basaltic and basaltic andesitic melts: An experimental and laser ICP-MS study with application to the oxidation state of mantle source regions. Earth and Planetary Science Letters, 392, 265–278.
Leeman, W.P., and Scheidegger, K.F. (1977) Olivine/liquid distribution coefficients and a test for crystal-liquid equilibrium. Earth and Planetary Science Letters, 35, 247–257.
Leitzke, F.P., Fonseca, R.O.C., Michely, L.T., Sprung, P., Münker, C., Heuser, A., and Blanchard, H. (2016) The effect of titanium on the partitioning behavior of high-field strength elements between silicates, oxides and lunar basaltic melts with applications to the origin of mare basalts. Chemical Geology, 440, 219–238.
Lin, Y., Tronche, E.J., Steenstra, E.S., and van Westrenen, W. (2017) Evidence for an early wet Moon from experimental crystallization of the lunar magma ocean. Nature Geoscience, 10, 14–18.
Liu, X., Xiong, X., Audétat, A., Li, Y., Song, M., Li, L., Sun, W., and Ding, X. (2014) Partitioning of copper between olivine, orthopyroxene, clinopyroxene, spinel, garnet and silicate melts at upper mantle conditions. Geochimica et Cosmochimica Acta, 125, 1–22.
Liu, X., Xiong, X., Audétat, A., and Li, Y. (2015) Partitioning of Cu between mafic minerals, Fe–Ti oxides and intermediate to felsic melts. Geochimica et Cosmochimica Acta, 151, 86–102.
Lodders, K. (2003) Solar system abundances and condensation temperatures of the elements. The Astrophysical Journal, 591, 1220–1247.
Longhi, J. (1977) Magma oceanography 2: Chemical evolution and crustal formation. Proceedings 8th Lunar Science Conference, 601–621.
Longhi, J., Walker, D., and Hays, J.F. (1978) The distribution of Fe and Mg between olivine and lunar basaltic liquids. Geochimica et Cosmochimica Acta, 42, 1545–1558.
Mallmann, G., and O'Neill, H.St.C. (2009) The crystal/melt partitioning of V during mantle melting as a function of oxygen fugacity compared with some other elements (Al, P, Ca, Sc, Ti, Cr, Fe, Ga, Y, Zr and Nb). Journal of Petrology, 50, 1765–1794.
——— (2013) Calibration of an empirical thermometer and oxybarometer based on the partitioning of Sc, Y and V between olivine and silicate melt. Journal of Petrology, 54, 933–949.
Martin, L.H.J., Schmidt, M.W., Mattsson, H.B., Ulmer, P., Hametner, K., and Gunther, D. (2012) Element partitioning between immiscible carbonatite-kamafugite melts with application to the Italian ultrapotassic suite. Chemical Geology, 320-321, 96–112. doi: 10.1016/j.chemgeo.2012.05.019
Matzen, A.K., Baker, M.B., Beckett, J.R., and Stolper, E.M. (2013) The temperature and pressure dependence of nickel partitioning between olivine and silicate melt. Journal of Petrology, 54, 2521–2545.
McDade, P., Blundy, J.D., and Wood, B.J. (2003) Trace element partitioning on the Tinaquillo Lherzolite solidus at 1.5 GPa. Physics of the Earth and Planetary Interiors, 139, 129–147.
McDonough, W.F., and Sun, S.-S. (1995) The composition of the Earth. Chemical Geology, 120, 223–253.
Mercer, C.N., and Johnston, A.D. (2008) Experimental studies of the P–T–H_2O near-liquidus phase relations of basaltic andesite from North Sister Volcano, High Oregon Cascades: constraints on lower-crustal mineral assemblages. Contributions to Mineralogy and Petrology, 155, 571–592.
Mikouchi, T., McKay, G., and Le, L. (1994) Cr, Mn, and Ca distributions for olivine in angritic systems: Constraints on the origins of Cr-rich and Ca-poor core olivine in angrite LEW87051. Lunar and Planetary Science, 25, 907–908.
Morgan, Z., Liang, Y., and Hess, P.C. (2006) An experimental study of anorthosite dissolution in lunar picritic magmas: implications for crustal assimilation processes. Geochimica et Cosmochimica Acta, 70, 3477–3491.
Newton, R.C., Anderson, A.T., and Smith, J.V. (1971) Accumulation of olivine in rock 12040 and other basaltic fragments in the light of analysis and syntheses. Proceedings 1st Lunar Science Conference, 575–582.
Ni, P., Zhang, Y., and Guan, Y. (2017) Volatile loss during homogenization of lunar melt inclusions. Earth and Planetary Science Letters, 478, 214–224.
Ni, P., Zhang, Y., Chen, S., and Gagnon, J. (2019) A melt inclusion study on volatile abundances in the lunar mantle. Geochimica et Cosmochimica Acta, 249, 17–41.
Nielsen, R.L., and Ustunisik, G.K. (2019) EarthChem Data. Olivine/melt partition coefficient experiments, version 1.0. Interdisciplinary Earth Data Alliance (IEDA), https://doi.org/10.1594/IEDA/111285.
Nielsen, R.L., Gallahan, W.E., and Newberger, F. (1992) Experimentally determined mineral-melt partition coefficients for Sc, Y and REE for olivine, orthopyroxene, pigeonite, magnetite and ilmenite. Contributions to Mineralogy and Petrology, 110, 488–499.
Nikogosian, I., and Sobolev, A. (1997) Ion-microprobe analysis of melt Inclusions in olivine: experience in estimating the olivine-melt partition coefficients of trace elements. Geochemistry International, 35, 119–126.
O'Neill, H.St.C., Berry, A.J., and Mallmann, G. (2018) The oxidation state of iron in Mid-Ocean Ridge Basaltic (MORB) glasses: Implications for their petrogenesis and oxygen fugacities. Earth and Planetary Science Letters, 504, 152–162.
Ottolini, L., Laporte, D., Raffone, N., Devidal, J.L., and Le, F., B. (2009) New experimental determination of Li and B partition coefficients during upper mantle partial melting. Contributions to Mineralogy and Petrology, 157, 313–325.
Papike, J.J., Karner, J.M., and Shearer, C.K. (2005) Comparative planetary mineralogy: Valence state partitioning of Cr, Fe, Ti, and V among crystallographic sites in olivine, pyroxene, and spinel from planetary basalts. American Mineralogist, 90, 277–290.
Papike, J.J., Burger, P.V., Bell, A.S., Le, L., Shearer, C.K., Sutton, S.R., Jones, J., and

Newville, M. (2013) Developing vanadium valence state oxybarometers (spinel-melt, olivine-melt, spinel-olivine) and V/(Cr+Al) partitioning (spinel-melt) for martian olivine-phyric basalts. American Mineralogist, 98, 2193–2196.
Pearce, N.J.G., Perkins, W.T., Westgate, J.A., Gorton, M.P., Jackson, S.E., Neal, C.R., and Chenery, S.P. (1997) A compilation of new and published major and trace element data for NIST SRM 610 and NIST SRM 612 Glass Reference Materials. Geostandards and Geoanalytical Research, 21, 115–144.
Rapp, J.F., and Draper, D.S. (2018) Fractional crystallization of the lunar magma ocean: updating the dominant paradigm. Meteoritics & Planetary Science, 53, 1432–1455.
Righter, K., Campbell, A.J., Humayun, M., and Hervig, R.L. (2004) Partitioning of Ru, Rh, Pd, Re, Ir, and Au between Cr-bearing spinel, olivine, pyroxene and silicate melts. Geochimica et Cosmochimica Acta, 68, 867–880.
Roeder, P.L., and Emslie, R.F. (1970) Olivine-liquid equilibrium. Contributions to Mineralogy and Petrology, 29, 275–289.
Rollinson, H.R. (1993) Using Geochemical Data: Evaluation, Presentation, Interpretation. Longman Scientific & Technical Press. Copublished in the U.S. with Wiley.
Rosenthal, A., Hauri, E.H., and Hirschmann, M.M. (2015) Experimental determination of C, F, and H partitioning between mantle minerals and carbonated basalt, CO_2/Ba and CO_2/Nb systematics of partial melting, and the CO_2 contents of basaltic source regions. Earth and Planetary Science Letters, 412, 77–87.
Salters, V.J., and Stracke, A. (2004) Composition of the depleted mantle. Geochemistry, Geophysics, Geosystems, 5, Q05004.
Salters, V.J.M., Longhi, J.E., and Bizimis, M. (2002) Near mantle solidus trace element partitioning at pressures up to 3.4 GPa. Geochemistry, Geophysics, Geosystems, 3, 1–23.
Sato, M., Hickling, N.L., and McLane, J.E. (1973) Oxygen fugacity values of Apollo 12, 14, and 15 lunar samples and reduced state of lunar magmas. Proceedings of the 4th Lunar Science Conference (Supplement 4, Geochimica et Cosmochimica Acta), 1061–1079.
Schreiber, H.D., and Haskin, L.A. (1976) Chromium in basalts: Experimental determination of redox states and partitioning among synthetic silicate phases. Proceedings of Lunar Science Conference, 7, 1221–1259.
Seifert, S., and Ringwood, A.E. (1988) The lunar geochemistry of chromium and vanadium. Earth, Moon and Planets, 40, 45–70.
Shannon, R.D. (1976) Revised effective ionic radii and systematic studies of interatomic distances in halides and chalcogenides. Acta Crystallographica, A32, 751–767.
Shearer, C.K., McKay, G., Papike, J.J., and Karner, J.M. (2006) Valence state partitioning of vanadium between olivine-liquid: Estimates of the oxygen fugacity of Y980459 and application to other olivine-phyric martian basalts. American Mineralogist, 91, 1657–1663.
Simon, S.B., and Sutton, S.R. (2017) Valence of Ti, V, and Cr in Apollo 14 aluminous basalts 14053 and 14072. Meteoritics & Planetary Science, 52, 2051–2066.
Sims, K.W.W., and DePaolo, D.J. (1997) Inferences about mantle magma sources from incompatible element concentration ratios in oceanic basalts. Geochimica et Cosmochimica Acta, 61, 765–784.
Snyder, G.A., Taylor, L.A., and Neal, C.R. (1992) A chemical model for generating the sources of mare basalts: Combined equilibrium and fractional crystallization of the lunar magmasphere. Geochimica et Cosmochimica Acta, 56, 3809–3823.
Spandler, C., and O'Neill, H.St.C. (2010) Diffusion and partition coefficients of minor and trace elements in San Carlos olivine at 1300 °C with some geochemical implications. Contributions to Mineralogy and Petrology, 159, 791–818.
Solomon, S.C., and Longhi, J. (1977) Magma oceanography: 1. thermal evolution. Proceedings of Lunar Science Conference, 8, 583–599.
Steele, I.M., and Smith, J.V. (1975) Minor elements in lunar olivine as a petrologic indicator. Proceedings of Lunar Science Conference, 6, 451–467.
Sun, C., and Liang, Y. (2013) The importance of crystal chemistry on REE partitioning between mantle minerals (garnet, clinopyroxene, orthopyroxene, and olivine) and basaltic melts. Chemical Geology, 358, 23–36.
Sutton, S.R., Jones, K.W., Gordon, B., Rivers, M.L., Bajt, S., and Smith, J.V. (1993) Reduced chromium in olivine grains from lunar basalt 15555: X-ray Absorption Near Edge Structure (XANES). Geochimica et Cosmochimica Acta, 57, 461–468.
Sutton, S.R., Karner, J., Papike, J., Delaney, J.S., Shearer, C., Newville, M., Eng, P., Rivers, M., and Dyar, M.D. (2005) Vanadium *K* edge XANES of synthetic and natural basaltic glasses and application to microscale oxygen barometry. Geochimica et Cosmochimica Acta, 69, 2333–2348.
Takahashi, E. (1978) Partitioning of Ni^{2+}, Co^{2+}, Fe^{2+}, Mn^{2+} and Mg^{2+} between olivine and silicate melts: compositional dependence of partition coefficient. Geochimica et Cosmochimica Acta, 42, 1829–1844.
Taura, H., Yurimoto, H., Kurita, K., and Sueno, S. (1998) Pressure dependence on partition coefficients for trace elements between olivine and the coexisting melts. Physics and Chemistry of Minerals, 25, 469–484.
Thomas, J.B., Bodnar, R.J., Shimizu, N., and Sinha, A.K. (2002) Determination of zircon/melt trace element partition coefficients from SIMS analysis of melt inclusions in zircon. Geochimica et Cosmochimica Acta, 66, 2887–2901.
Toplis, M.J., and Carroll, M.R. (1995) An experimental study of the influence of oxygen fugacity on Fe-Ti oxide stability, phase relations, and mineral—Melt equilibria in ferro-basaltic systems. Journal of Petrology, 36, 1137–1170.
Usselman, T.M., Lofgren, G.E., Donaldson, C.H., and Williams, R.J. (1975) Experimentally reproduced textures and mineral chemistries of high-titanium mare basalts. Proceedings of Lunar Science Conference, 6, 997–1020.
Wadhwa, M. (2008) Redox conditions on small bodies, the Moon and Mars. Reviews in Mineralogy and Geochemistry, 68, 493–510.
Walker, D., Kirkpatrick, R.J., Longhi, J., and Hays, J.F. (1976) Crystallization history of lunar picritic basalt sample 12002: Phase-equilibria and cooling-rate studies. Geological Society of America Bulletin, 87, 646–656.
Wang, Z., and Gaetani, G.A. (2008) Partitioning of Ni between olivine and siliceous eclogite partial melt: experimental constraints on the mantle source of Hawaiian basalts. Contributions to Mineralogy and Petrology, 156, 661–678.
Wood, B.J., Smythe, D.J., and Harrison, T. (2019) The condensation temperatures of the elements: A reappraisal. American Mineralogist, 104, 844–856.
Wood, B.J., Wade, J., and Kilburn, M.R. (2008) Core formation and the oxidation state of the Earth: Additional constraints from Nb, V and Cr partitioning. Geochimica et Cosmochimica Acta, 72, 1415–1426.
Wood, J.A., Dickey, J.S., Marvin, U.B., and Powell, B.N. (1970) Lunar anorthosites and a geophysical model of the Moon. Proceedings Apollo 11 Lunar Science Conference, 965–988.
Xirouchakis, D., Hirschmann, M.M., and Simpson, J.A. (2001) The effect of titanium on the silica content and on mineral-liquid partitioning of mantle-equilibrated melts. Geochimica et Cosmochimica Acta, 65, 2201–2217.
Yu, Y., Zhang, Y., Chen, Y., and Xu, Z. (2016) Kinetics of anorthite dissolution in basaltic melt. Geochimica et Cosmochimica Acta, 179, 257–274.
Zajacz, Z., and Halter, W. (2007) LA-ICPMS analyses of silicate melt inclusions in co-precipitated minerals: Quantification, data analysis and mineral/melt partitioning. Geochimica et Cosmochimica Acta, 71, 1021–1040.
Zhang, Y., Ni, H., and Chen, Y. (2010) Diffusion data in silicate melts. Reviews in Mineralogy and Geochemistry, 72, 311–408.

Manuscript received January 13, 2021
Manuscript accepted July 29, 2021
Manuscript handled by Chiara Maria Petrone

Endnote:

[1]Deposit item AM-22-87971, Online Materials. Deposit items are free to all readers and found on the MSA website, via the specific issue's Table of Contents (go to http://www.minsocam.org/MSA/AmMin/TOC/2022/Aug2022_data/Aug2022_data.html).